SUPPORTING INFORMATION FOR

Non-Linear Photo-switching in Molecular Actuators through Intra-molecular Energy Transfer from an Electron Donating Core

*Óscar Guzmán-Méndez [a], Emmanuel Villatoro [a,†], Mariana M. Reza [a], Maria Eugenia Sandoval [a,‡], Jesus Jara-Cortés [b], Martha Elena García-Aguilera [a], Melissa Bravo-Romero [a], José G. López-Cortés [a], and Jorge Peon [a,]**

[a] Instituto de Química, Universidad Nacional Autónoma de México, Ciudad de México, México.

[b] Unidad Académica de Ciencias Básicas e Ingenierías, Universidad Autónoma de Nayarit, Tepic, Nayarit, México.

[†]Present Address: Department of Chemistry, Northwestern University, Evanston, Illinois 60208, United States.

[‡]Present Address: Department of Physical Chemistry, University of Alicante, E-03080 Alicante, Spain.

*Corresponding author

Table of Contents

List of Figures and Tables

Synthesis procedures and characterization data

Azo-I: (E)-2-((4-iodophenyl)diazenyl)-1-methyl-1H-pyrrole

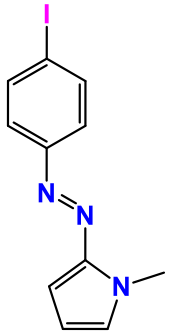

A round-bottomed flask was charged with acetone (15 mL), water (15 mL), 4-iodoaniline (2.1 g, 9.6 mmol), concentrated HCl (13 mL), and cooled to 0°C. Subsequently, $NaNO_2$ (0.77 g, 10.64 mmol) was dissolved in water was added dropwise. After an hour, a mixture of acetone (15 mL), water (15 mL), and N-methylpyrrole (0.65 g, 8.0 mmol) and Na_2CO_3 (1.7 g, 16 mmol), was transferred slowly into the flask. The mixture was left stirring for another hour. Then, acetone was removed under vacuum and the aqueous mixture was extracted with ethyl acetate. The organic phase was dried over sodium sulfate and evaporated. The product was then recrystallized from EtOH as dark orange crystals. (2.27g, 7.3 mmol, 91% yield). ^{1}H NMR (500 MHz, d6-DMSO) δ 7.86 (d, J = 8.6 Hz, 2H, H_8), 7.55 (d, J = 8.6 Hz, 2H, H_7), 7.33 (t, J = 2.1 Hz, 1H, H_2), 6.65 (dd, J = 4.2, 1.7 Hz, 1H, H_4), 6.31 (dd, J = 4.2, 2.6 Hz, 1H, H_3), 3.92 (s, 3H, H_1). HRMS [DART]: calculated for $C_{11}H_{11}IN_3$ $[M+H]^+$: 311.99976, found: 311.99977.

pp-4I: 1,4-bis(4-iodophenyl)-2,5-bis(4-nitrophenyl)-1,4-dihydropyrrolo[3,2-b]pyrrole

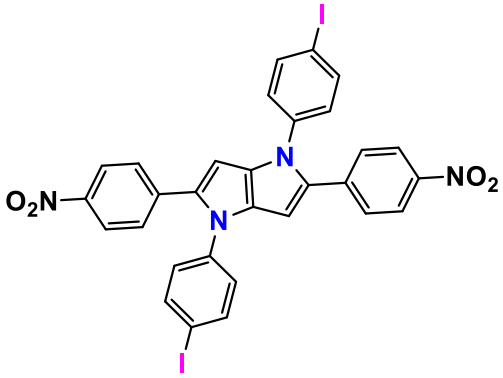

One-step protocol: Adapting one of the optimized protocols from Gryko et al.,[1,2] a round-bottom flask was charged with 4-iodoaniline (1095 mg, 5mmol), 4-nitrobenzaldehyde (755 mg, 5 mmol), 2,3-butanedione (215 mg, 2.5 mmol), iron(III) acetylacetonate (105.9 mg) and 8 mL of 1:1 toluene/acetic acid. The reaction was heated at 50 °C for over 24 h. TLC analysis showed a complex mixture of spots. The product was purified via silica gel flash chromatography with DCM/hexane as eluent. The product was isolated as an orange solid (600 mg, 34% yield).

Two-step protocol: First, 4-iodoaniline (440 mg, 2mmol) and 4-nitrobenzaldehyde (302 mg, 2mmol) were charged into a round-bottom flask with 10 mL of EtOH under reflux for 2h. The imine formed was filtered off as yellow precipitate and dried over a vacuum (610 mg, 1.7 mmol). The imine was then dissolved in 5 mL 1:1 toluene/acetic acid along with butanedione (74 mg, 0.85 mmol) and p-toluensulfonic acid (28mg, 0.17 mmol). The reaction was heated at

50 °C for 24 h. Afterward, the product slowly precipitates out of the solution. The product is filtered and washed with EtOH and obtained as an orange solid (330 mg, 46% global yield).

Three-step protocol: 4-iodoaniline (440 mg, 2mmol) and 4-nitrobenzaldehyde (302 mg, 2mmol) were charged into a round-bottomed flask with 10 ml of EtOH and set to reflux for 2h. The imine formed was filtered off as yellow precipitate and dried over a vacuum (630 mg, 1.78 mmol). The imine (600 mg, 1.7 mmol) was then dissolved in 5 ml of 1:1 toluene/acetic acid along with butanedione (74 mg, 0.85 mmol) and p-toluensulfonic acid (28mg, 0.17 mmol). The reaction was set at 50°C for 24h. Afterward, the solvent is evaporated and replaced with 7 mL MeCN. Next, solid DDQ (470 mg, 2.0 mmol) was added, and the mixture refluxed over 24h. The product is filtered off the solution, washed with EtOH and dry over a vacuum (480 mg, 64% global yield). ^{1}H NMR (500 MHz, $CDCl_3$) δ 6.54 (s, 1H, H_6), 7.02 (d, *J* = 8.66 Hz, 2H, H_3), 7.33 (d, *J* = 9.07 Hz, 2H, H_9), 7.76 (d, *J* = 8.67 Hz, 2H, H_2), 8.12 (d, *J* = 8.92 Hz, 2H, H_{10}). ^{13}C NMR (126 MHz, $CDCl_3$) δ 145.85, 138.92, 138.86, 138.77, 135.08, 133.53, 127.85, 127.04, 123.94, 97.18, 91.51. HRMS (FAB$^+$): Calculated for $C_{30}H_{18}N_4O_4I_2$ [M^+] 751.9418, found 751.9421.

pp-3I: 1,3-bis(3-iodophenyl)-2,5-bis(4-nitrophenyl)-1,4-dihydropyrrolo[3,2-b]pyrrole

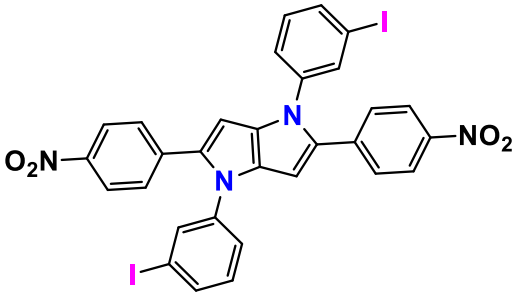

For convenience, the 2-step protocol previously described for **pp-4I** was followed. First, 3-iodoaniline (760 mg, 3.5 mmol) and 4-nitrobenzaldehyde (524 mg, 3.5 mmol) were charged into a round-bottom flask with 10 mL of EtOH and set to reflux for 2h. The imine formed was filtered off as yellow precipitate and dried over vacuum (1120 mg, 3.1 mmol). The imine was then dissolved in 10 mL of 1:1 toluene/acetic acid along with butanedione (135 mg, 1.56 mmol) and p-toluensulfonic acid (52 mg, 0.3 mmol). The reaction was heated at 50 °C for over 24 h. Afterward, the product slowly precipitates out of the solution. The product is filtered and washed with EtOH as an orange solid (510 mg, 43% global yield). ^{1}H NMR (500 MHz, Chloroform-*d*) δ 6.48 (s, 1H, H_8), 7.07 (m, 2H, $H_{5,2}$), 7.27 (d, *J* = 9.14 Hz, 2H, H_{11}), 7.62 (m, 1H, H_1), 7.66 (m, 1H, H_3), 8.05 (d, *J* = 8.93 Hz, 2H, H_{12}).^{13}C NMR (126 MHz, $CDCl_3$) δ 145.8, 140.19, 138.86, 136.03, 135.21, 133.94, 133.62, 131.03, 127.89, 124.93, 123.92, 97.26, 94.51. HRMS (FAB$^+$): Calculated for $C_{30}H_{18}N_4O_4I_2$ [M^+] 751.9418, found 751.9419.

For the syntheses of **pp-3sap** and **pp-4sap**, a protocol was employed where first the corresponding pyrrolopyrrole di-iodo derivative was synthesized. Subsequently, a Mizoroki-Heck coupling reaction formed the vinyl terminal derivative (**pp-nH**, where n=3 or 4) and finally these compounds were coupled with **Azo-I** to obtain the respective product. The synthetic details are written in Experimental Section. Below are detailed experimental procedures for the different synthetic steps to produce **pp-bap** beginning from the hydrogenation of the 4-nitrophenylboronic acid pinacol, followed the formation of the respective imine, and continued with the reaction to form the pyrrolo-pyrrole core. The Suzuki-Miyaura cross coupling reaction procedure to form **pp-bap** was described in the Experimental Section.

4-(4,4,5,5-tetramethyl-1,3,2-dioxaborolan-2-yl)aniline.

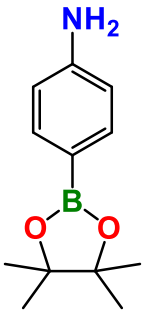

To a methanol solution of 4-nitrophenylboronic acid pinacol (500 mg, 2.0 mmol, 1.0 eq.), 53 mg of Pd/C 10% w/w were added under a nitrogen atmosphere. This reaction media was kept under vigorous stirring and at room temperature for ten minutes. After this, a hydrogen balloon was connected to the flask. Every fifteen minutes the reaction mixture was monitored by TLC until the nitro compound disappeared. The crude was filtered by celite under vacuum. A grey pale solid was obtained as a precipitate (420 mg, 1.92 mmol, 96% yield). ^{1}H NMR (500 MHz, $CDCl_3$) δ 1.33 (s, 12H; H_3), 3.84 (s, 2H; broad signal), 6.66 (dt, *J* = 8.57, 2.11, 2.01 Hz, 2H; H_1), 7.63 (dt, *J* = 8.58, 1.95, 1.75 Hz, 2H; H_2). ^{13}C NMR (126 MHz, $CDCl_3$) δ 24.88, 83.33, 114.11, 136.44, 149.37 (Note: the carbon attached to boron was not observed due to quadrupole broadening caused by the ^{11}B nucleus). HRMS (DART) calculated for $C_{12}H_{18}BNO_2$ $[M+H]^+$ 220.15088, found 220.15117.

((E)-1-(4-nitrophenyl)-N-(4-(4,4,5,5-tetramethyl-1,3,2-dioxaborolan-2-yl)phenyl)methanimine).

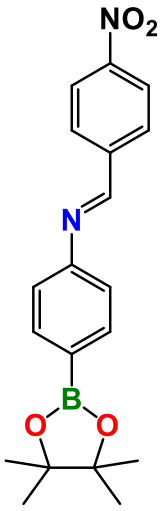

A round bottom flask was prepared with an ethanolic solution of the corresponding aniline (219 mg, 1.0 mmol, 1.0 eq.) and heated to 50°C, 4-nitrobenzaldehyde solid was added slowly (151 mg, 1.0 mmol, 1.0 eq.). The reaction mixture was left under stirring and reflux for 2 hours until a yellow solid precipitated from the solution (172 mg, 0.488 mmol, 49% yield). ^{1}H NMR (500 MHz, $CDCl_3$) δ 1.36 (s, 12H; H_6), 7.23 (dt, *J* = 8.48, 2.00, 1.59 Hz, 2H; H_4), 7.87 (dt, *J* = 8.28, 1.80, 1.70 Hz, 2H; H_5), 8.08 (dt, *J* = 8.79, 2.17, 1.90 Hz, 2H; H_2), 8.33 (dt, *J* = 8.75, 2.10, 1.87 Hz, 2H; H_1), 8.54 (s, 1H; H_3). ^{13}C NMR (126 MHz, $CDCl_3$) δ 24.89, 83.94, 120.22, 124.05, 129.53, 136.02, 141.46, 149.37, 153.49, 157.96 (Note: the carbon attached to boron was not observed due to quadrupole broadening caused by ^{11}B nucleus). HRMS (DART) calculated for $C_{19}H_{21}BN_2O_4$ $[M+H]^+$ 353.16726, found 353.16583.

pp-boo:2,5-bis(4-nitrophenyl)-1,4-bis(4-(4,4,5,5-tetramethyl-1,3,2-dioxaborolan-2-yl)phenyl)-1,4-dihydropyrrolo[3,2-b]pyrrole

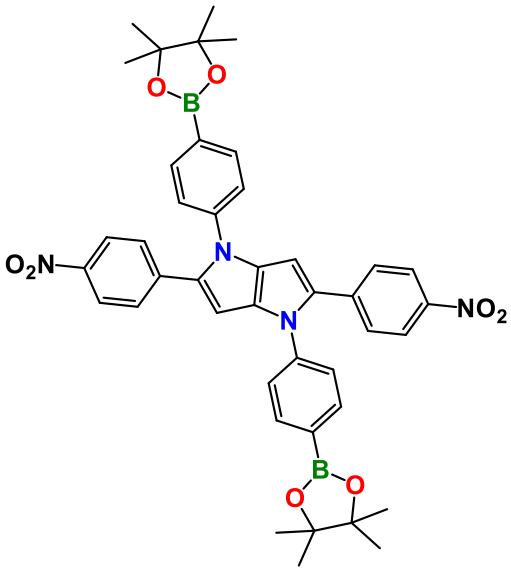

A round-bottomed flask was charged with 235 mg (0.667 mmol, 1.0 eq.) of the corresponding imine, which was suspended in 5 mL of dry acetonitrile. Dropwise (33 mg, 0.367 mmol, 0.55 eq.), 2,3-butanedione was added. This solution was left at room temperature for 24 hours. The reaction mixture evolved into a dark suspension and was poured into an ice bath, filtered, and washed with cold acetonitrile. A crystalline orange solid was obtained (148 mg, 0.197 mmol, 59% yield). ^{1}H NMR (500 MHz, $CDCl_3$) δ 1.37 (s, 24H, H_6), 6.56 (s, 2H; H_3), 7.26 (dt, *J* = 8.43, 1.85, 1.53 Hz, 4H; H_4), 7.31 (dt, *J* = 9.00, 2.43, 1.97 Hz, 4H; H_2), 7.87 (dt, *J* = 8.43, 1.74, 1.55 Hz, 4H; H_5), 8.08 (dt, *J* = 11.47, 2.44, 1.81 Hz, 4H; H_1). ^{13}C NMR (126 MHz, $CDCl_3$) δ 24.92, 84.15, 97.31, 123.84, 124.49, 127.83, 133.76, 135.10, 136.19, 139.36, 141.53, 145.64 (Note: the carbon attached to boron was not observed due to quadrupole

broadening caused by ^{11}B nucleus). HRMS (DART) calculated for $C_{42}H_{42}B_2N_4O_8$ $[M+H]^+$ 753.32670, found 753.32439.

Azo-Br: (E)-2-((4-bromophenyl)diazenyl)-1-methyl-1H-pyrrole.

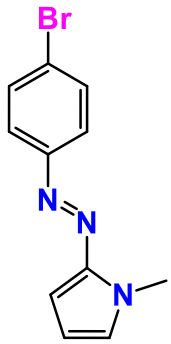

A round-bottomed flask was charged with 887 mg of 4-bromoaniline (5.0 mmol, 1.0 eq.) which were previously dissolved in 5 mL of HPLC methanol. This solution was poured into an ice bath at 0 °C with stirring. 10 mL HCl 6.0 M was added to the former solution. After 10 minutes, an aqueous solution of $NaNO_2$ (414 mg, 6.0 mmol, 1.2 eq.) was added dropwise. Simultaneously, 406 mg N-methylpyrrole (5.0 mmol, 1.0 eq.) and 2 mL NEt_3 were mixed into a second flask, which was poured under an ice bath. After 30 minutes, the basic solution with N-methylpyrrole was slowly added to the first solution. The reaction mixture was left at room temperature. The compound was purified by silica gel column chromatography, using hexanes 100% as eluent. ^1H NMR (500 MHz, $CDCl_3$) δ 3.96 (s, 3H, H_6), 6.31 (dd, *J* = 2.69, 1.60 Hz, 1H, H_4), 6.73 (dd, *J* = 2.61, 1.58, 1.57 Hz, 1H, H_3), 6.96 (t, *J* = 12.57, 2.06, 1.98 Hz, 1H, H_5), 7.57 (dt, *J* = 8.88, 2.67, 1.95 Hz, 2H, H_2), 7.68 (dt, *J* = 8.73, 2.61, 2.05 Hz, 1H, H_1). ^{13}C NMR (126 MHz, $CDCl_3$) δ 33.48, 100.60, 110.56, 123.14, 123.49, 127.48, 132.12, 146.42, 152.39. HRMS (DART) calculated for $C_{11}H_{10}BrN_3$ $[M+H]^+$ 264.01363, found 264.01388.

pp-ophen:

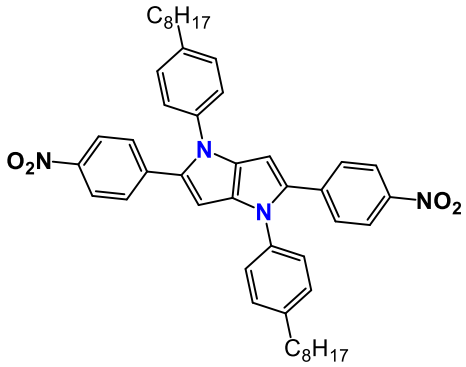

The synthesis of this molecule followed the method by Gryko *et al.*[2] This pyrrole-pyrrole was synthesized from 5 mmol 4-nitrobenzaldehyde, 5 mmol 4-octylaniline, 2.5 mmol 2,3-butanedione in 5 mL of glacial acetic acid. Finally, 85 mg dry p-toluensulfonic acid (10% mol), which was previously. The reaction mixture was kept at 90°C for 3 hours. The mixture was cooled and neutralized with NaOH/water to pH=7.0. The reaction crude was washed with water and recrystallized with chloroform. A crystalline orange solid was obtained, filtered off and washed with cold acetonitrile (0.60 g, 33% yield). ^1H NMR (500 MHz, $CDCl_3$) δ 0.82 (d, *J* = 6.95 Hz, 6H, H_{13}), 1.25 (m, 20H; $H_{8\text{-}12}$), 1.59 (m, 4H, H_7), 2.58 (t, *J* = 7.79 Hz, 4H, H_6), 6.46 (s, 2H, H_3), 7.12 (dt, *J* = 8.51, 1.85, 1.77 Hz, 4H, H_5), 7.15 (dt, *J* = 8.29, 2.06, 1.66 Hz, 4H, H_4), 7.25

(dt, *J* = 8.97, 2.40, 1.96 Hz, 4H, H_2), 7.99 (dt, *J* = 8.89, 2.44, 1.76 Hz, 4H, H_1), ^{13}C NMR (125 MHz, $CDCl_3$) δ 14.14, 22.69, 29.29, 29.37, 31.36, 31.90, 35.53, 96.42, 123.72, 125.28, 127.64, 129.58, 134.08, 135.21, 136.78, 139.62, 141.91, 145.47.

NMR Spectra

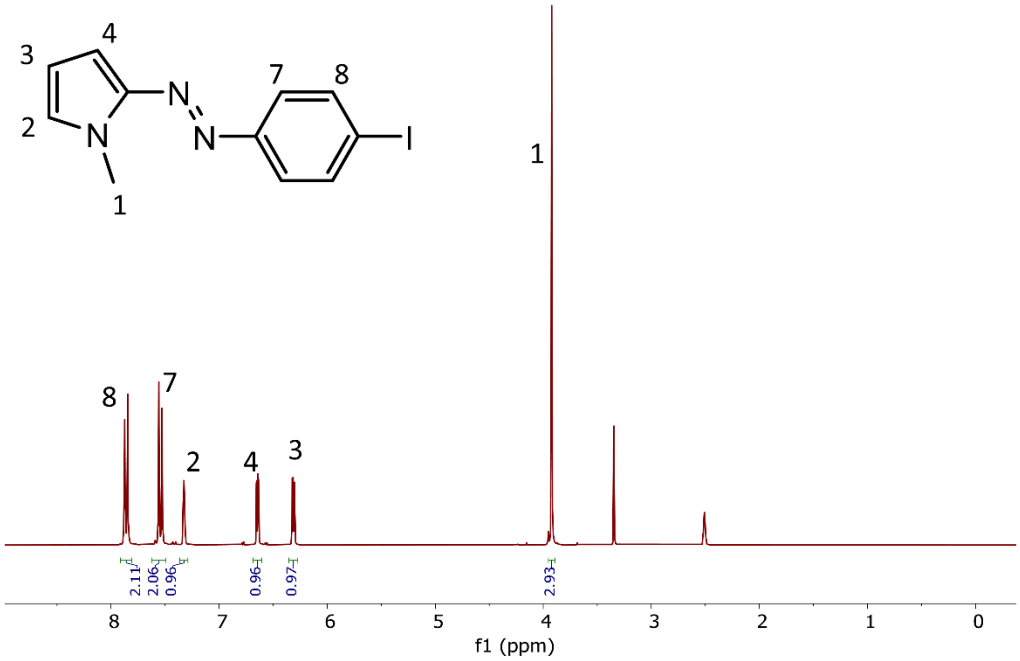

Figure S1: ^{1}H NMR spectrum (500 MHz, d6-DMSO) of **Azo-I**.

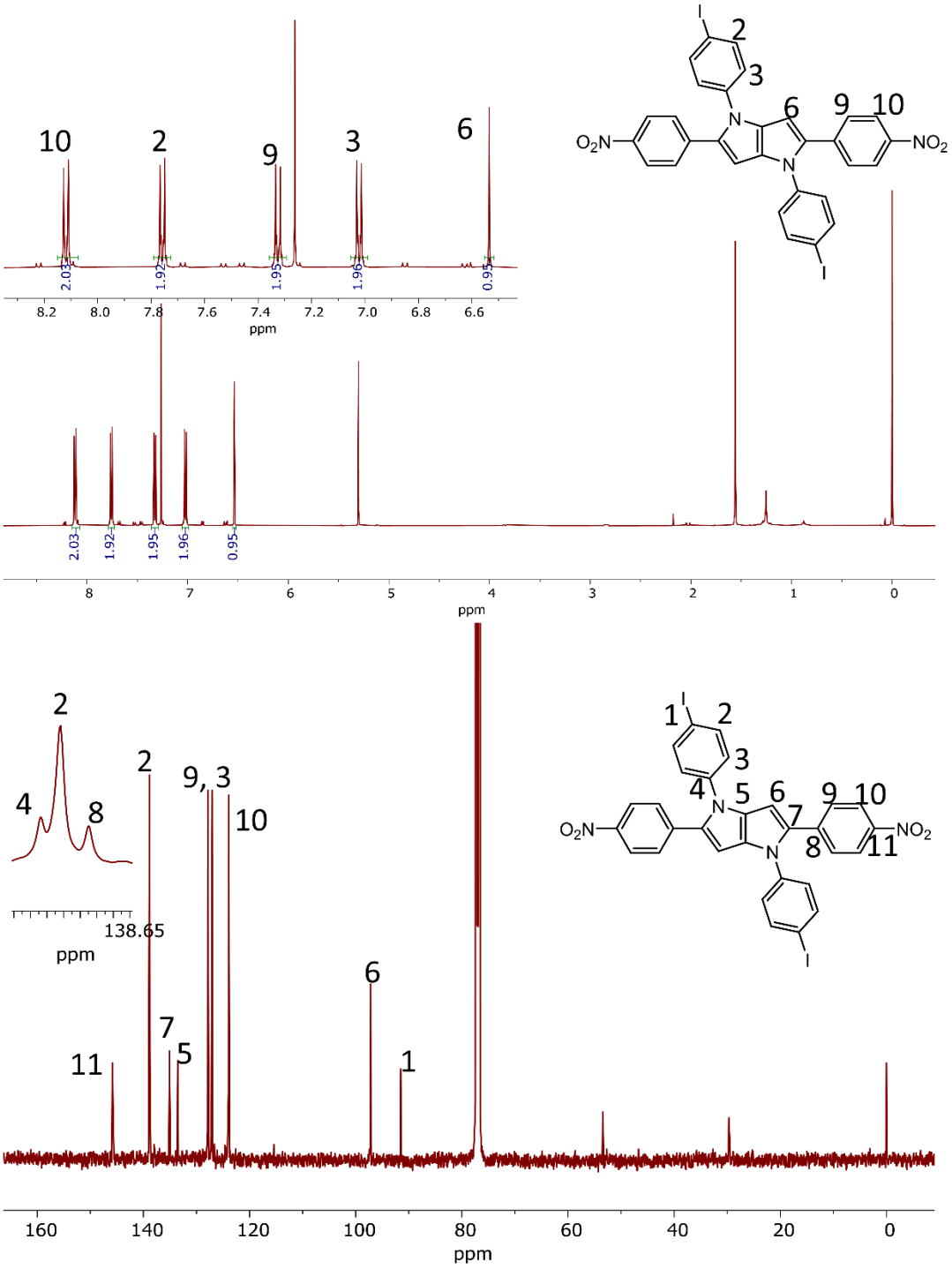

Figure S2. NMR spectra of **pp-4I**. Top: ^{1}H NMR spectrum (500 MHz, $CDCl_3$). Bottom: ^{13}C NMR spectrum (125 MHz, $CDCl_3$).

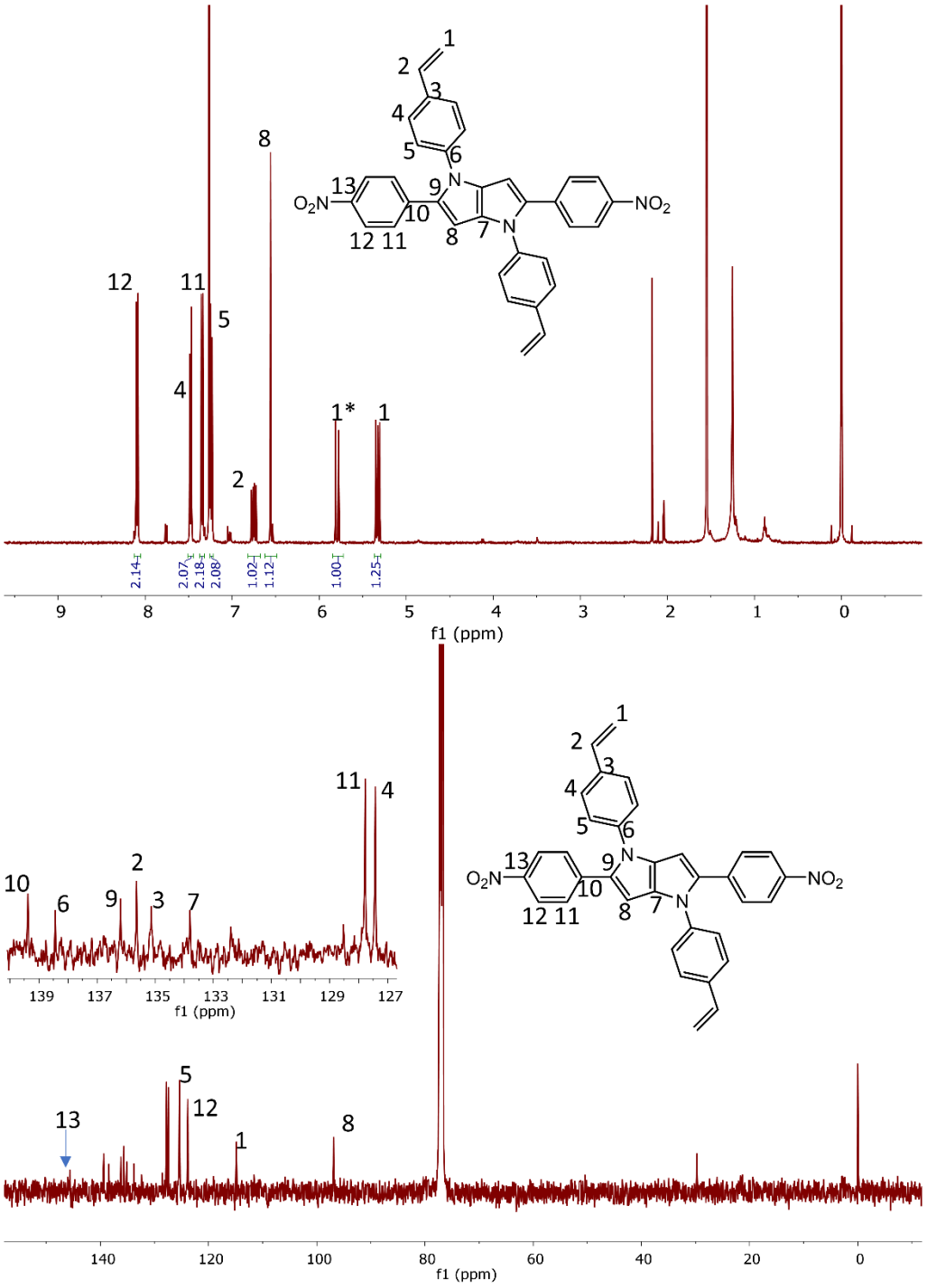

Figure S3. NMR spectra of **pp-4H**. Top: ^{1}H NMR spectrum (500 MHz, $CDCl_3$). Bottom: ^{13}C NMR spectrum (125 MHz, $CDCl_3$).

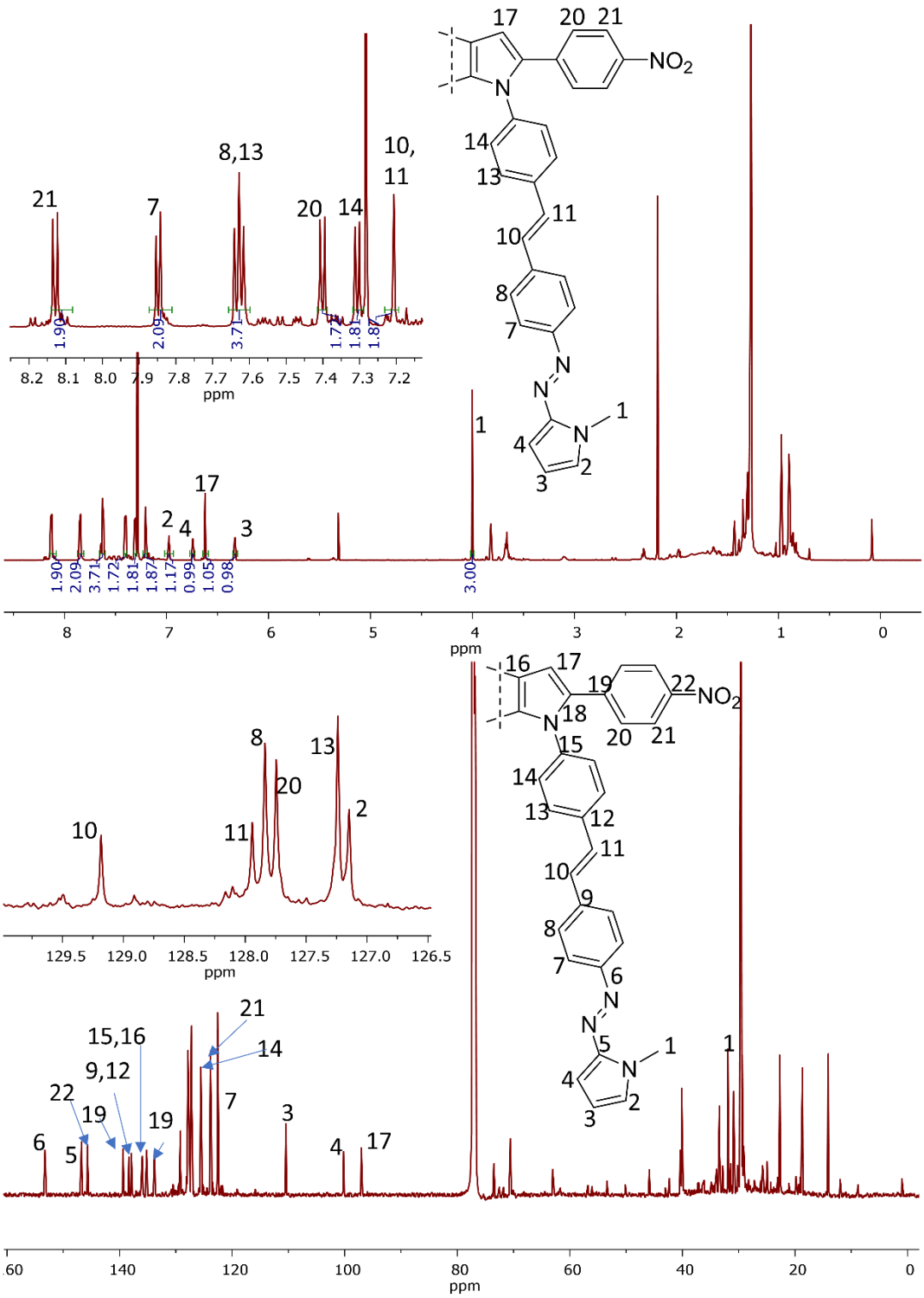

Figure S4. NMR spectra of **pp-4sap**. Top: ^{1}H NMR spectrum (500 MHz, $CDCl_3$). Bottom: ^{13}C NMR spectrum (125 MHz, $CDCl_3$).

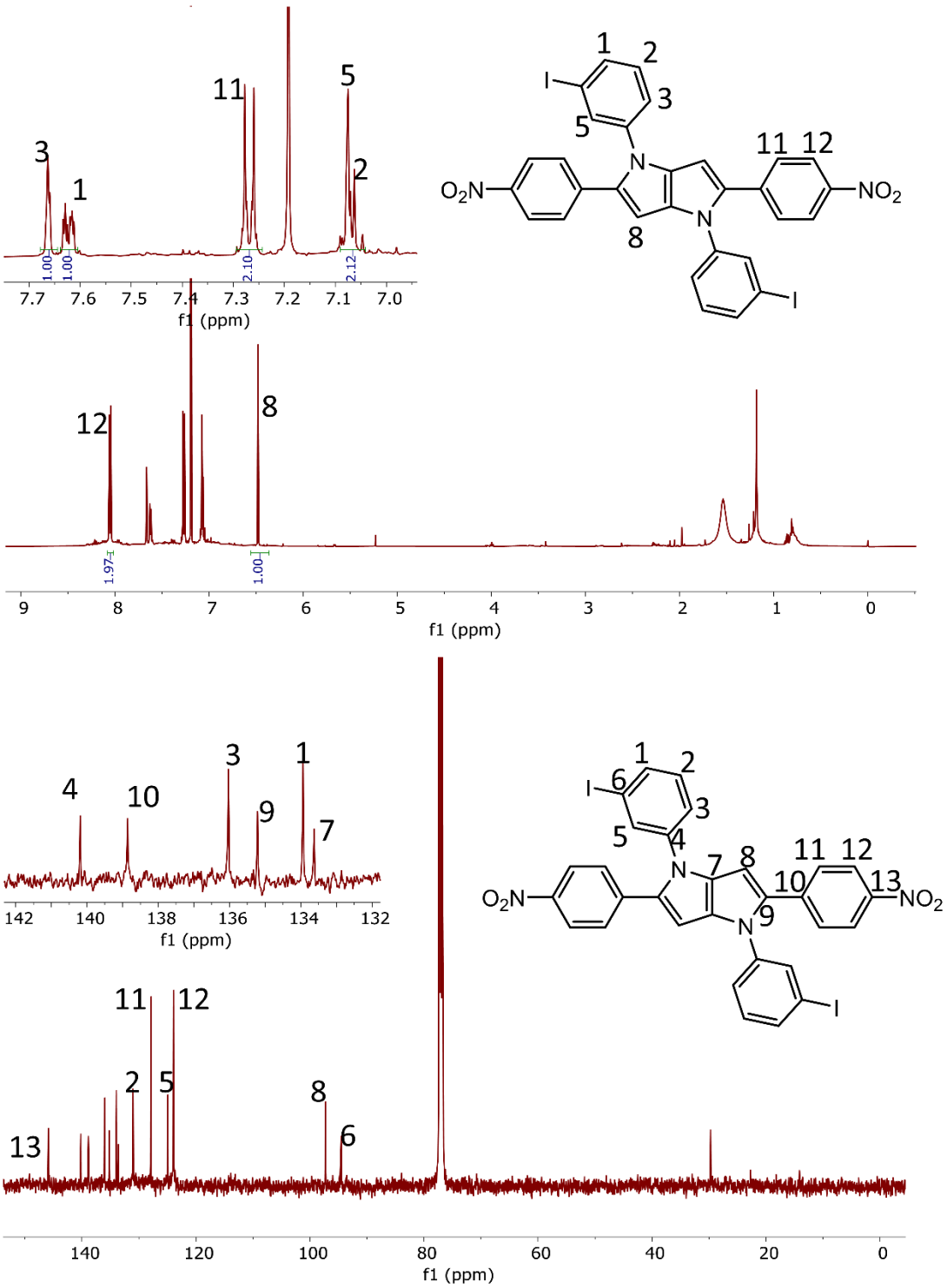

Figure S5. NMR spectra of **pp-3I**. Top: ^{1}H NMR spectrum (500 MHz, $CDCl_3$). Bottom: ^{13}C NMR spectrum (125 MHz, $CDCl_3$).

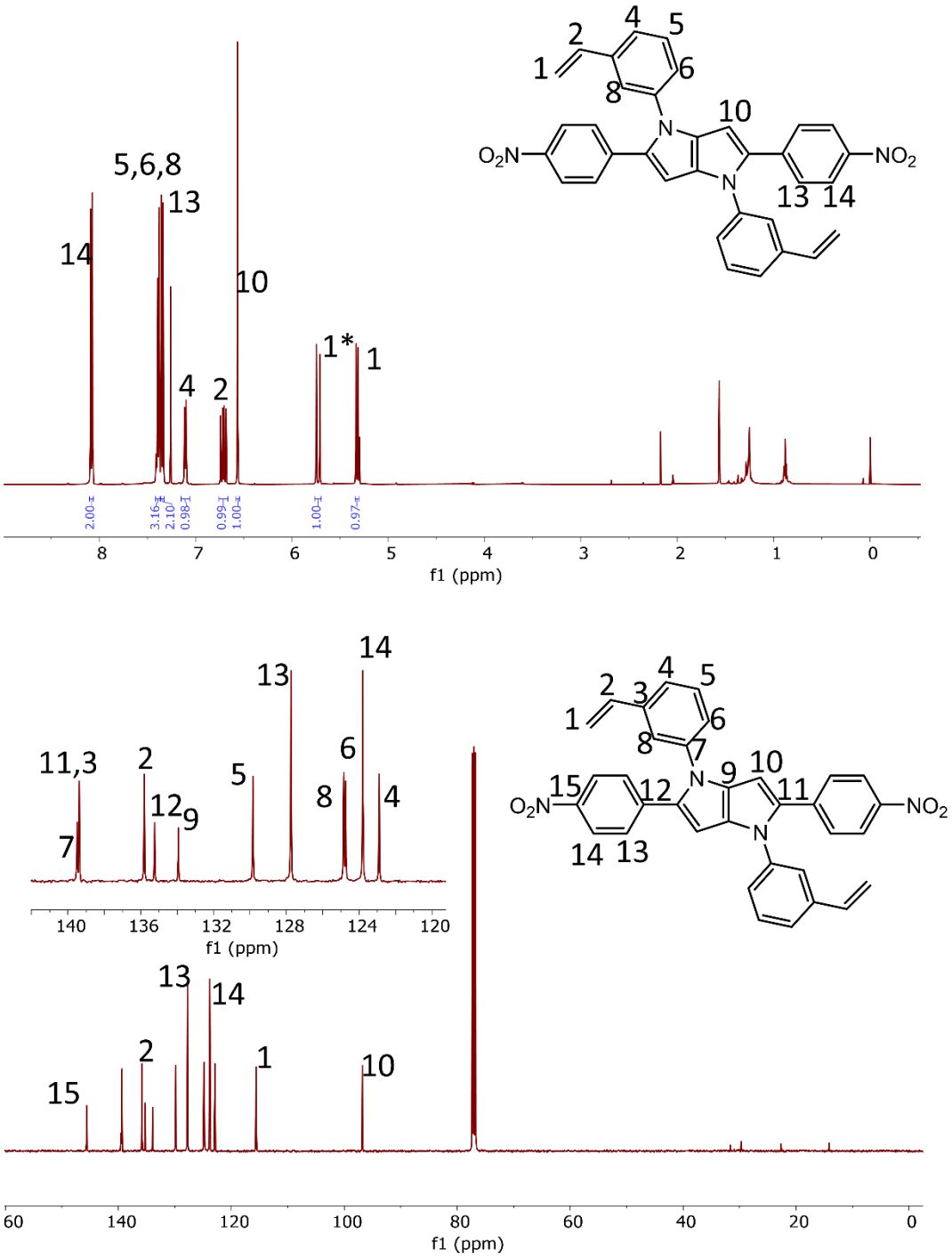

Figure S6. NMR spectra of **pp-3H**. Top: ^{1}H NMR spectrum (500 MHz, $CDCl_3$). Bottom: ^{13}C NMR spectrum (125 MHz, $CDCl_3$).

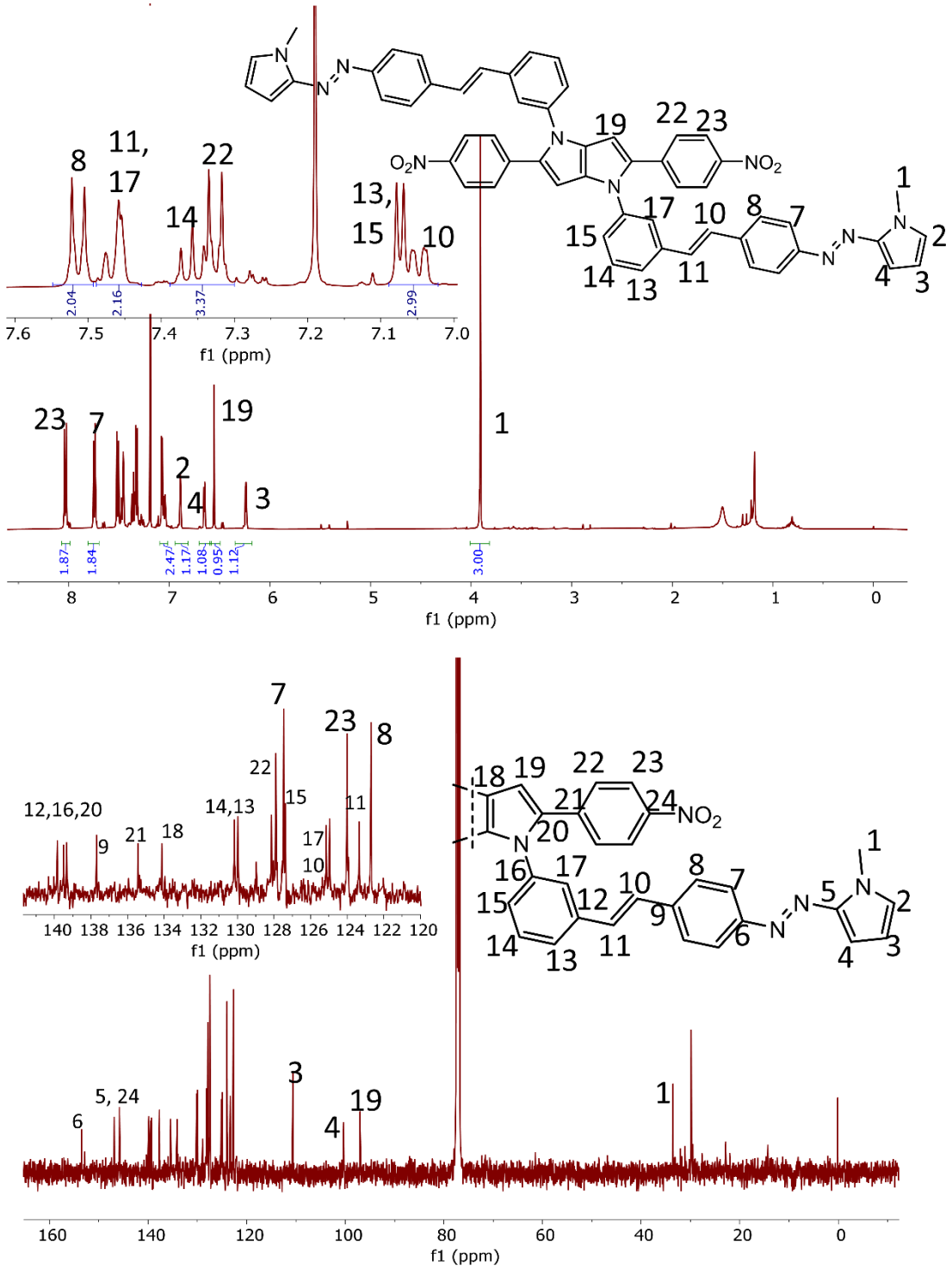

Figure S7. NMR spectra of **pp-3sap**. Top: ^{1}H NMR spectrum (500 MHz, $CDCl_3$). Bottom: ^{13}C NMR spectrum (125 MHz, $CDCl_3$).

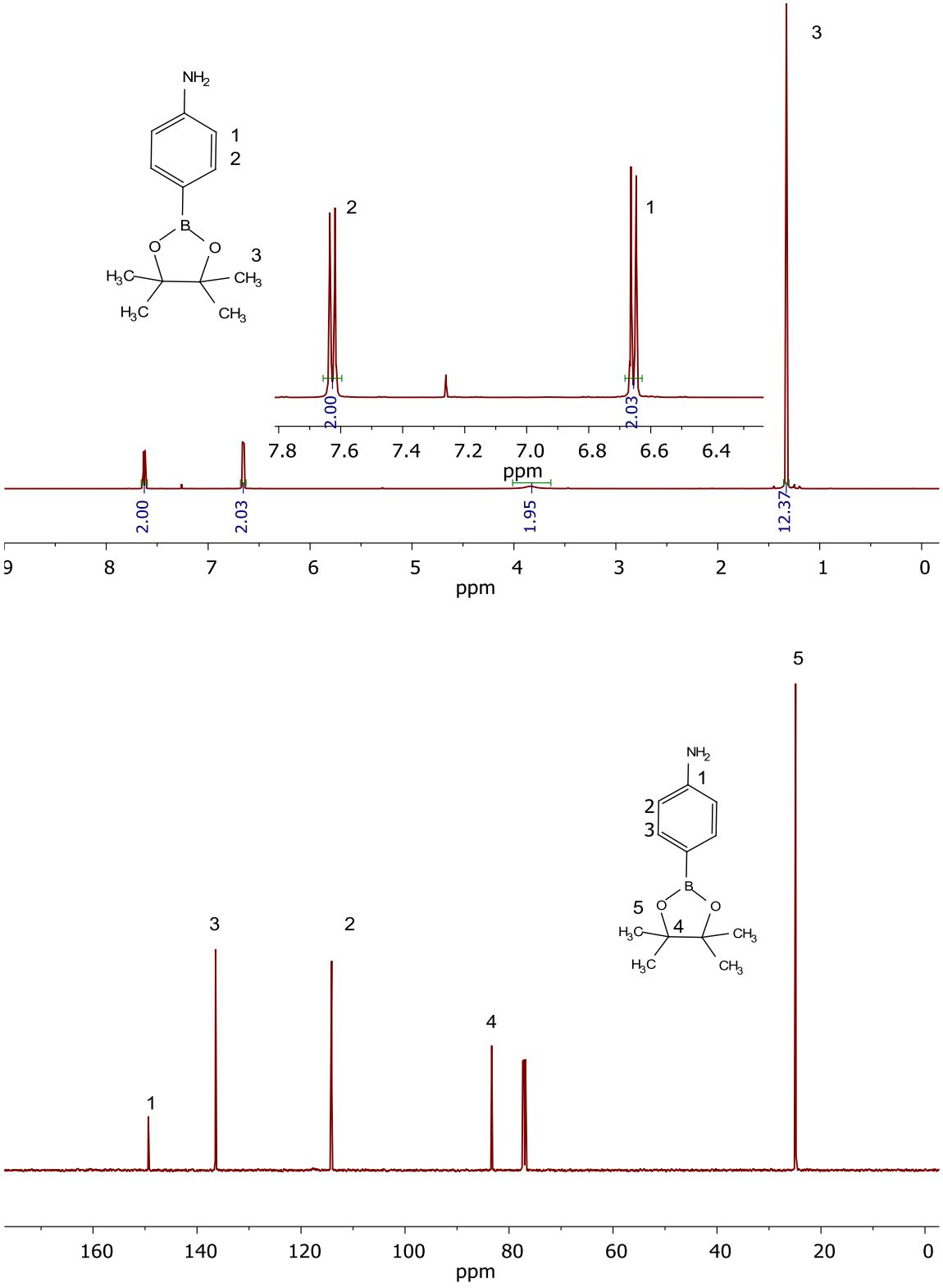

Figure S8. NMR spectra of **4-aminophenyl pinacol boronic acid**. Top: ^{1}H NMR spectrum (500 MHz, $CDCl_3$). Bottom: ^{13}C NMR spectrum (125 MHz, $CDCl_3$).

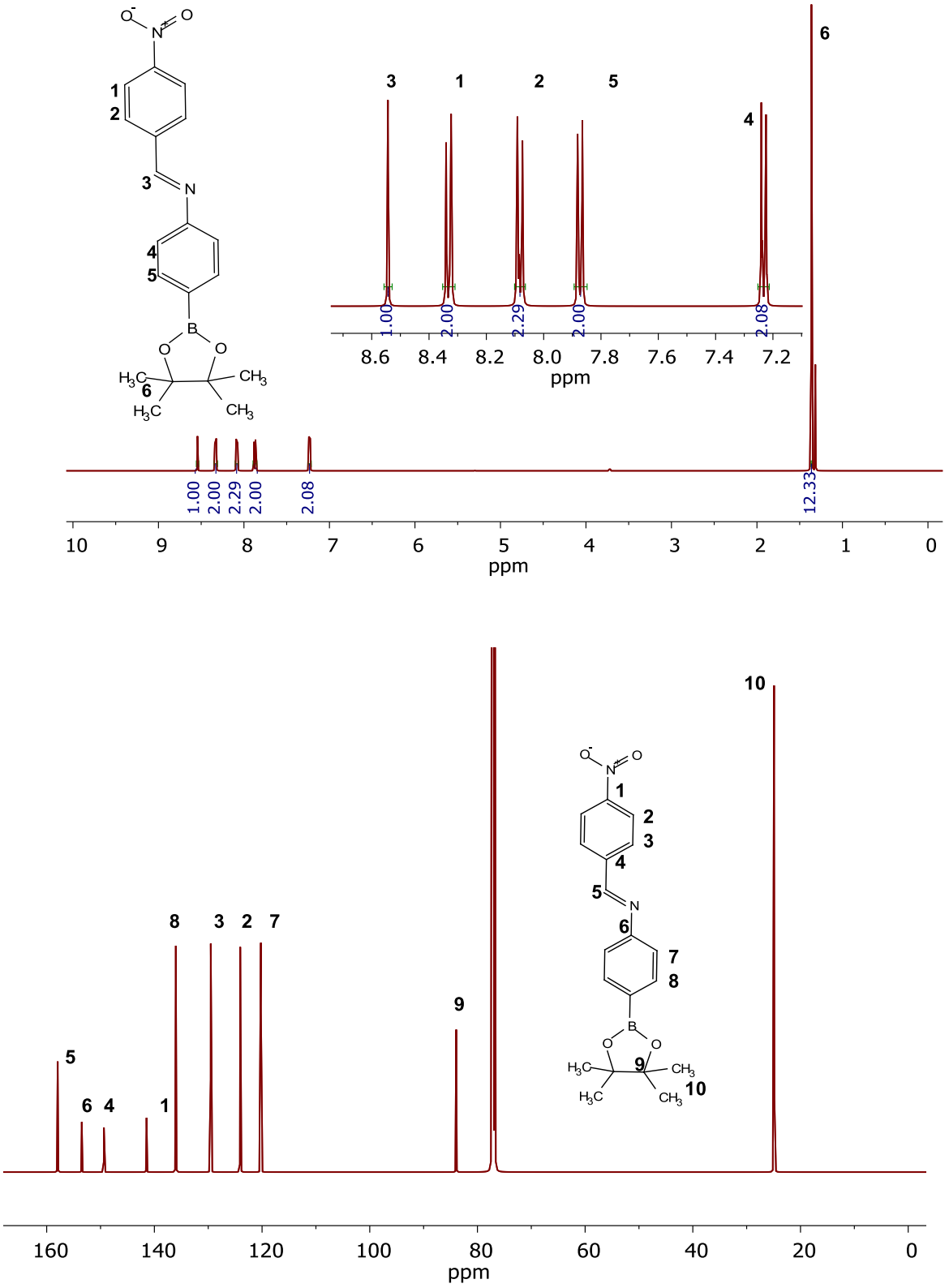

Figure S9. NMR spectra of imine derived from **4-aminophenyl pinacol boronic acid**. Top: ^{1}H NMR spectrum (500 MHz, $CDCl_3$). Bottom: ^{13}C NMR spectrum (125 MHz, $CDCl_3$).

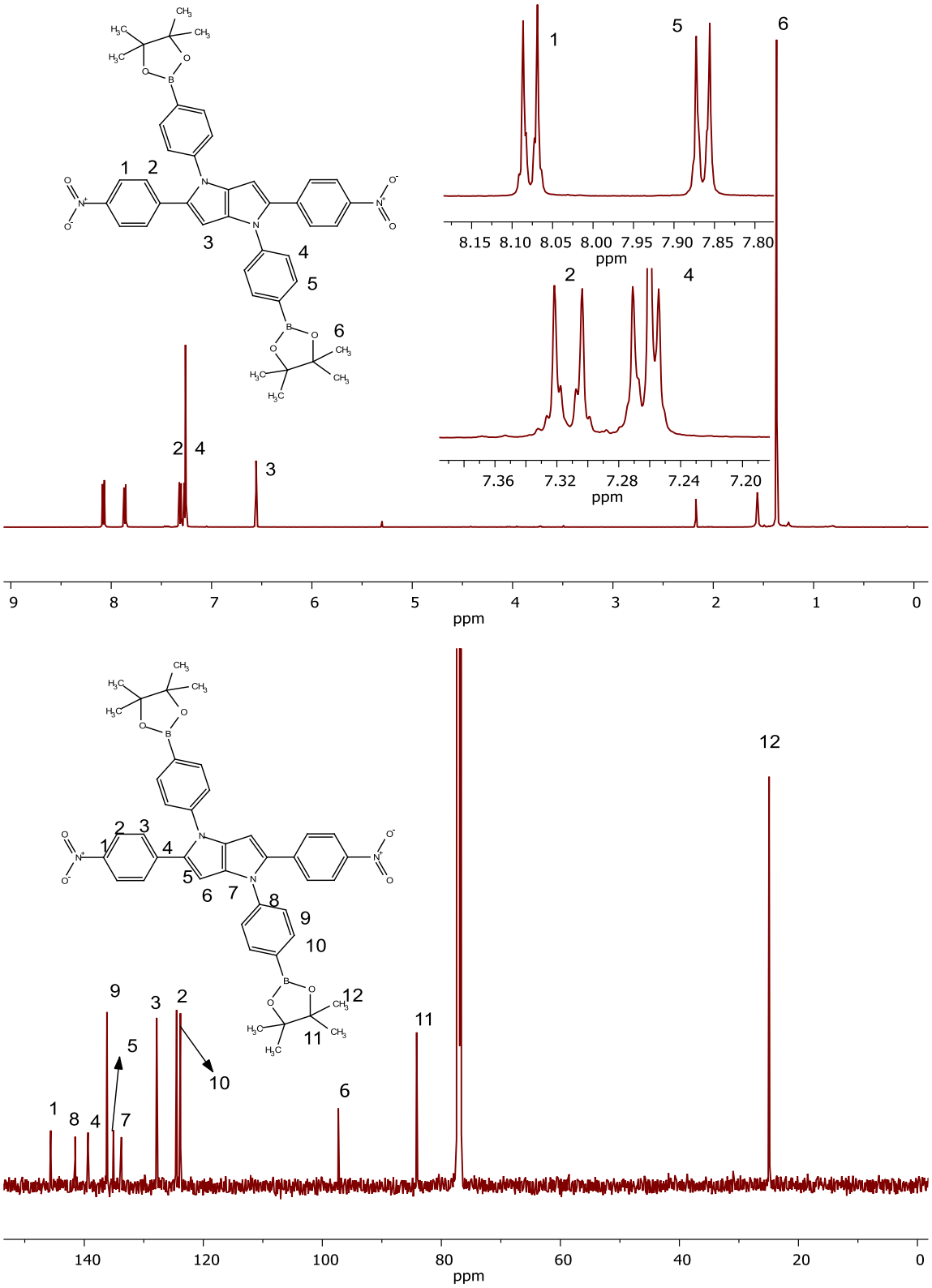

Figure S10. NMR spectra of **pp-boo**. Top: ^{1}H NMR spectrum (500 MHz, $CDCl_3$). Bottom: ^{13}C NMR spectrum (125 MHz, $CDCl_3$).

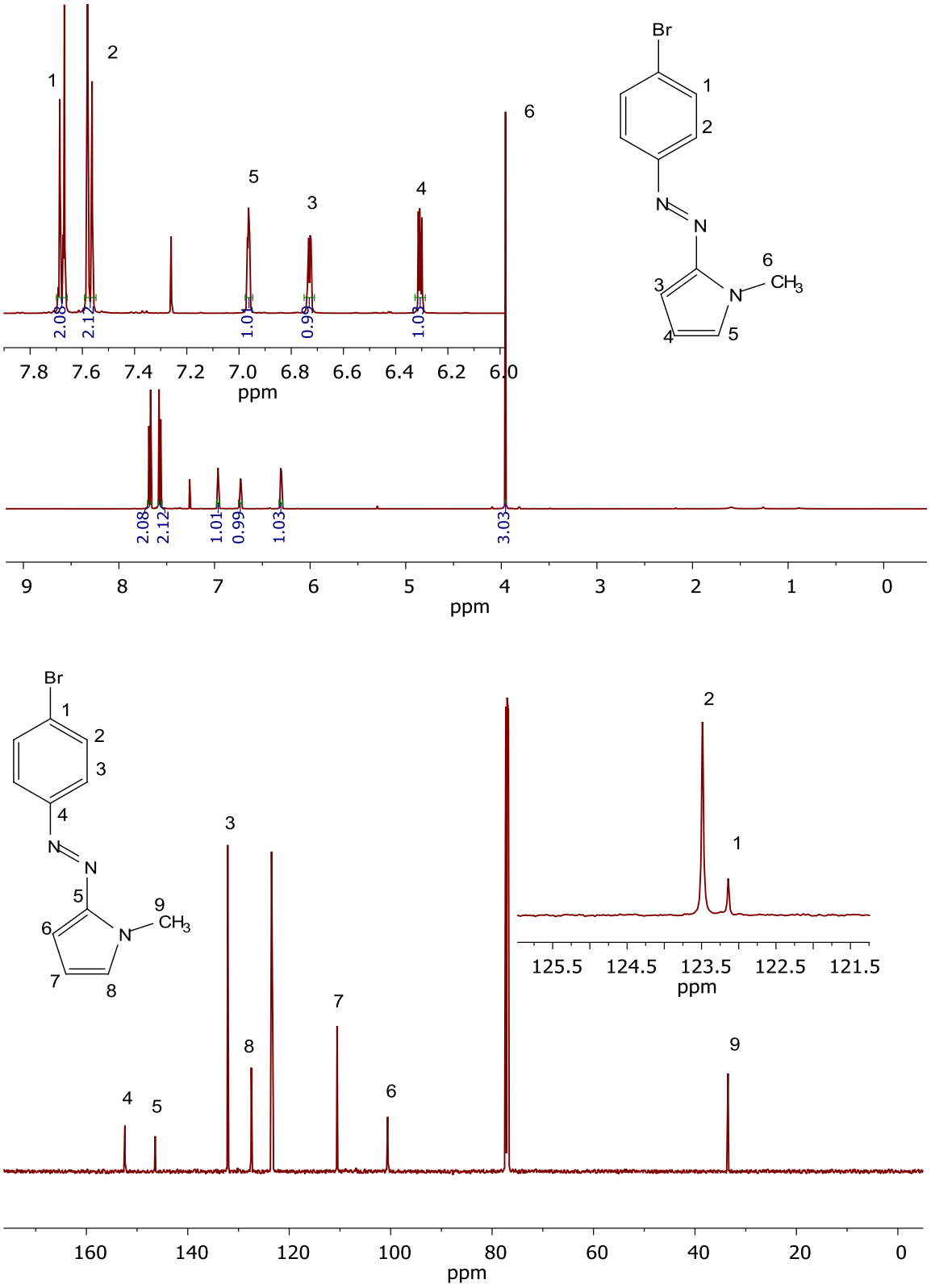

Figure S11. NMR spectra of **Azo-Br**. Top: ^{1}H NMR spectrum (500 MHz, $CDCl_3$). Bottom: ^{13}C NMR spectrum (125 MHz, $CDCl_3$).

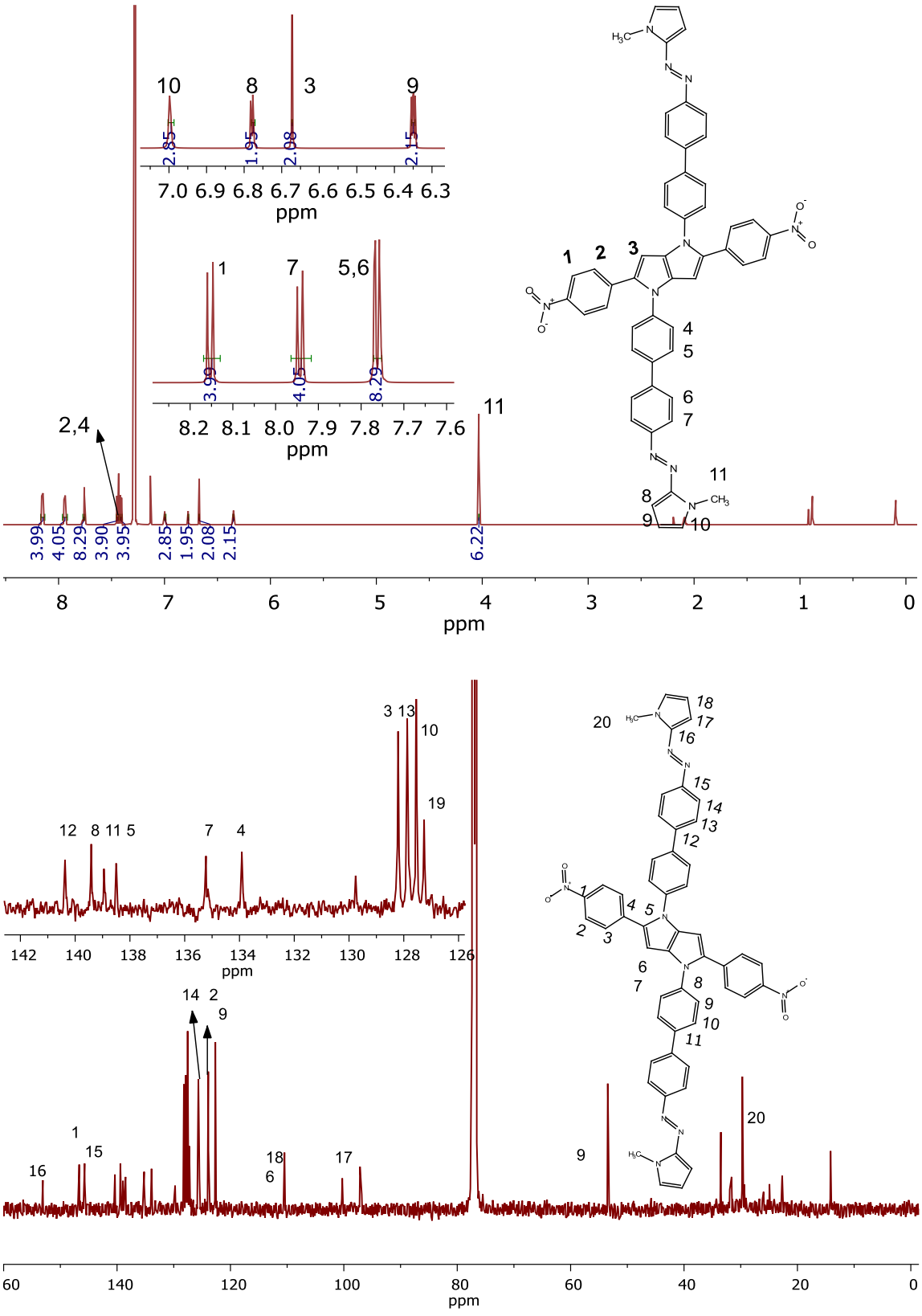

Figure S12. NMR spectra of **pp-bap**. Top: ^{1}H NMR spectrum (500 MHz, $CDCl_3$). Bottom: ^{13}C NMR spectrum (125 MHz, $CDCl_3$).

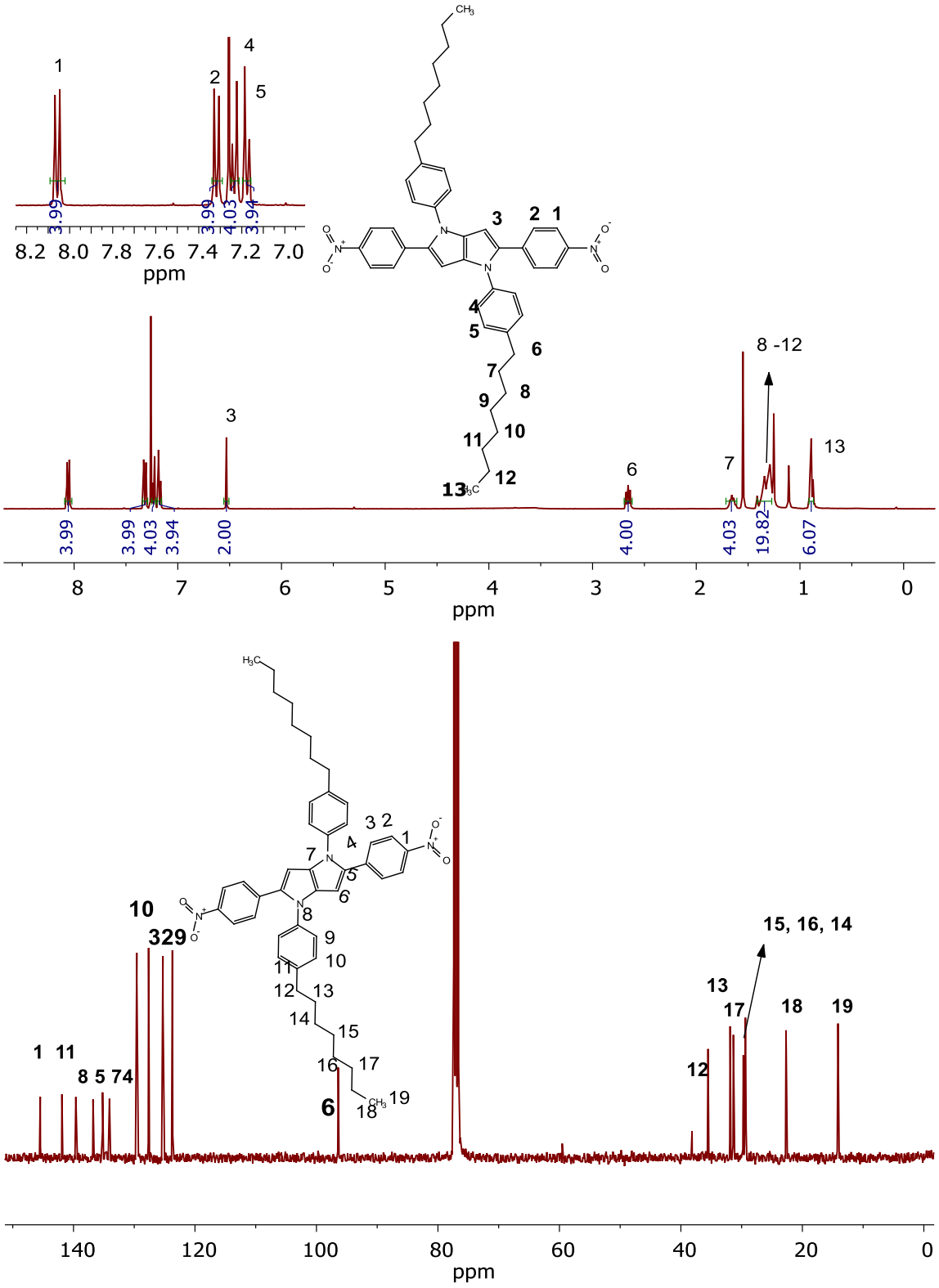

Figure S13. NMR spectra of **pp-ophen**. Top: ^{1}H NMR spectrum (500 MHz, $CDCl_3$). Bottom: ^{13}C NMR spectrum (125 MHz, $CDCl_3$).

Photochemical Transformation of pp-bap by NMR

The figure below illustrates how the ^{1}H-NMR signals of **pp-bap** are modified from the *E*-*Z* isomerization in an actuator arm after linear photo-excitation with a 450 nm laser at 5 mW power for 5 seconds in deuterated chloroform solution at room temperature. The respective UV-Vis evolution in this solvent is shown in Figure S28. First, the singlet at 4.03 ppm (s) corresponds to the protons of the N- methyl group of the *E*-isomer terminal actuator. After irradiation, this singlet shows a reduction in its intensity (indicated by a blue down-arrow), and a new singlet appears (at 4.11 ppm indicated by a red up-arrow). This new singlet is assigned to the protons of N-methyl group of the photo-induced *Z*-isomer in one of the actuator arms.

Additionally, the signals assigned to the three different protons directly bonded to the terminal pyrrole at 7.00 (t), 6.78 (d,d) and 6.35 ppm (d,d) show a decrease in their relative intensity upon irradiation and correspondingly three new signals emerge. These new signals are localized at 6.86, 6.00 and 4.92 ppm (marked by red up-arrows). As another example, the singlet at 6.67 ppm (s) is assigned to the proton of pyrrolo-pyrrole core (see H3 in the top spectrum in Figure S12) and decreases upon irradiation. Concurrently, a slightly shifted signal emerges (red up-arrow at 6.66 ppm). The emergence of new signals and the decrease in the relative intensity in those associated to the protons of the *E*-isomer demonstrates a change in the geometry of one of the actuators arms towards the *Z*-form in **pp-bap** upon irradiation.

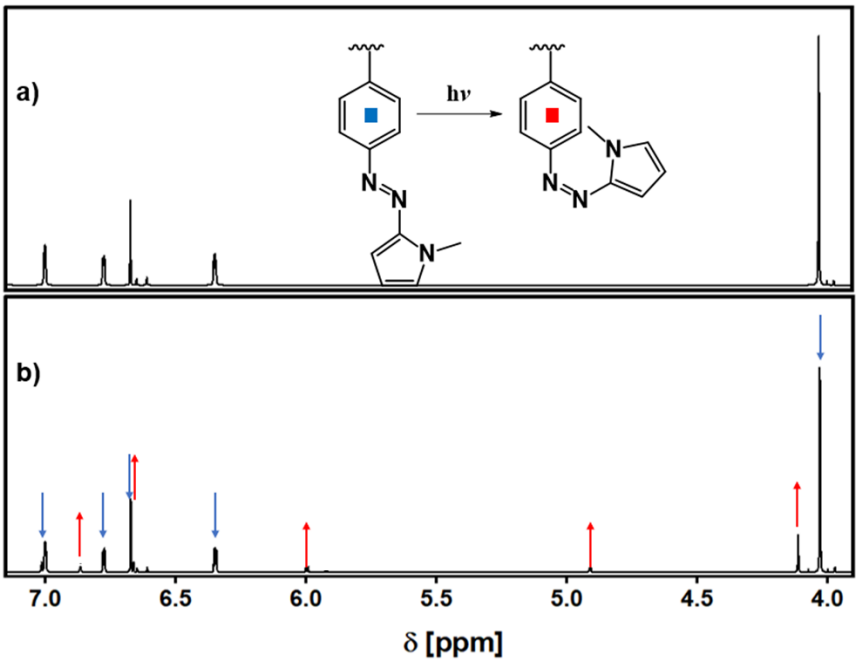

Figure S14. ^{1}H-NMR spectra (700 MHz) of **pp-bap** in $CDCl_3$ solution at 21 °C. a) Spectrum before the irradiation, and b) spectrum after the irradiation (only 5 seconds with a 450 nm laser at 5 mW power).

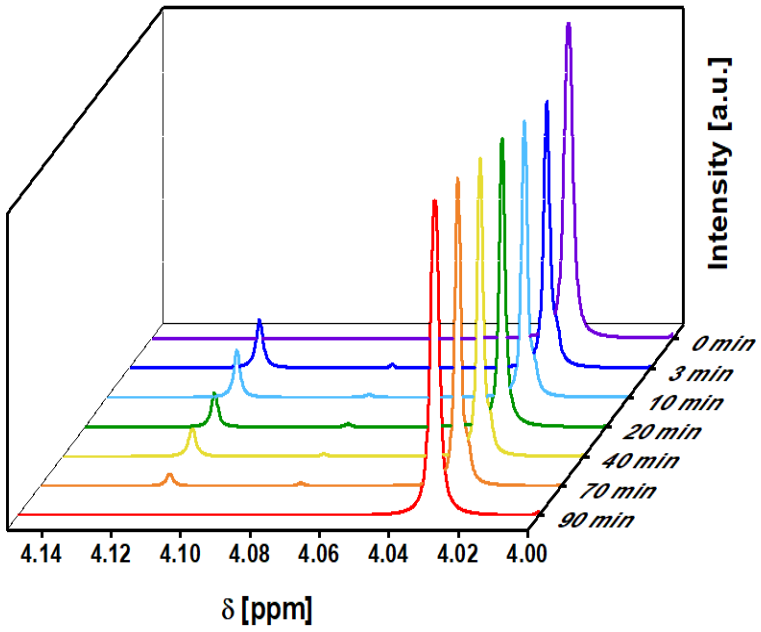

Figure S15. ^{1}H-NMR spectra (700 MHz) of **pp-bap** in $CDCl_3$ solution at 21 °C showing the thermal *Z*⟶*E* back-isomerization for the azo bond after 450 nm irradiation. The top spectrum (purple) corresponds to before irradiation. The blue spectrum exhibits a decrease of the singlet at 4.03 ppm upon irradiation and the emergence of a second singlet at 4.11 pm indicating the formation of the *Z*-isomer as indicated in Figure S14. The rest of the spectra shows the evolution of these two singlet signals as a function of time. Finally, the red spectrum shows the entire back-transformation to the initial form as the singlet at 4.11 ppm vanishes completely.

Computational Results

Table S1. Calculated vertical transition energies, oscillator strengths (*f*) and TPA cross sections (σ_2, GM) for the low-energy singlet excited states of **pp-3sap**. Information about the transition character and nature is included (localized: LE, charge transfer: CT, mixed excitation: ME), together with the TD-DFT orbital amplitudes. The parentheses indicate if the transition is associated with a localized transition (pp: at the core, sap: at the actuators), or if the transition has a charge transfer character.

State	ΔE [eV]	*f*	σ_2 [GM]	Character	Nature	TD-DFT Weights	Amplitude Conf.
S_1	2.354	0.025	2.51	$^1\pi\pi^*$	CT (sap→pp)	0.62	H → L
S_2	2.363	0.006	7.76	$^1\pi\pi$*	CT (sap→pp)	0.32 0.61	H-1 → L+1 H-1 → L
S_3	2.457	1.271	2.42	$^1n\pi$*	LE (pp)	0.69	H-2 → L
S_4	2.509	0.000	0.02	$^1n\pi$*	LE (sap)	0.47 -0.40 0.26	H-4 → L+3 H-4 → L+2 H-5 → L+2
S_5	2.509	0.000	0.02	$^1\pi\pi^*$	LE (sap)	0.47 0.40 0.26	H-5 → L+3 H-5 → L+2 H-4 → L+2
S_6	2.704	2.288	1070.00	$^1\pi\pi^*$	LE (sap)	0.49 0.46	H → L+2 H-1 → L+3
S_7	2.710	0.564	71.90	$^1\pi\pi^*$	ME	0.41 -0.37 -0.36	H-2 → L+1 H-1 → L+2 H → L+3
S_8	2.781	0.385	921.00	$^1\pi\pi^*$	ME	0.45 0.35 0.32	H-2 → L+1 H → L+3 H-1 → L+2
S_9	2.815	0.182	1.44	$^1\pi\pi^*$	CT (sap→pp)	-0.50 0.40	H -3 → L H-1 → L+1

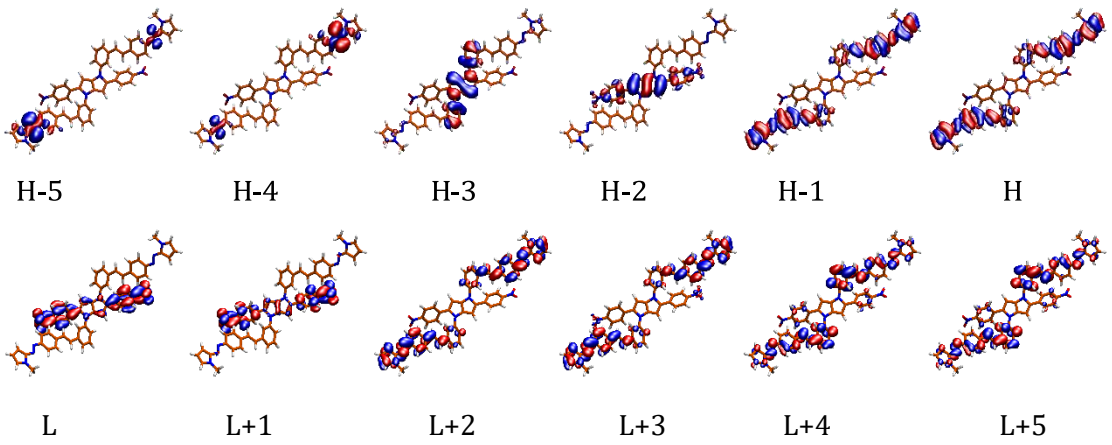

Figure S16. Iso-surface of the molecular orbitals involved in the description of the low energy singlet electronic states of **pp-3sap**.

Table S2. Calculated vertical transition energies, oscillator strengths (*f*) and TPA cross sections (σ_2, GM) for the low-energy singlet excited states of **pp-4sap**. Information about the transition character and nature is included (localized: LE, charge transfer: CT, mixed excitation: ME), together with the TD-DFT orbital amplitudes. The parentheses indicate if the transition is associated with a localized transition (pp: at the core, sap: at the actuators), or if the transition has a charge transfer character.

State	ΔE [eV]	*f*	σ_2 [GM]	Character	Nature	TD-DFT Weights	Amplitude Conf.
S_1	2.408	1.410	0.37	$^1\pi\pi^*$	CT (sap→pp)	0.56 0.39	H → L H-2 → L
S_2	2.505	0.676	0.76	$^1\pi\pi$*	LE (pp)	0.58 -0.35	H-2 → L H → L
S_3	2.509	0.005	0.30	$^1n\pi$*	LE (sap)	0.50 0.41	H-2 → L H-2 → L
S_4	2.510	0.001	0.59	$^1n\pi$*	LE (sap)	0.50 -0.42	H-5→ L+1 H-5 → L+2
S_5	2.555	0.001	455.00	$^1\pi\pi^*$	CT (sap→pp)	0.64	H → L+2
S_6	2.637	3.325	1.83	$^1\pi\pi^*$	LE (sap)	0.54 -0.40	H → L+2 H-1 → L+1
S_7	2.663	0.007	410.00	$^1\pi\pi^*$	LE (sap)	0.41 -0.41 -0.28	H → L+1 H-1 → L+2 H → L+3
S_8	2.778	0.001	1480.00	$^1\pi\pi^*$	ME	0.45 0.34 0.26 0.26	H → L+3 H → L+1 H-2 → L+1 H-2 → L+3
S_9	2.825	0.012	642.00	$^1\pi\pi^*$	CT (pp→sap)	0.60 -0.27	H-2 → L+1 H → L+3

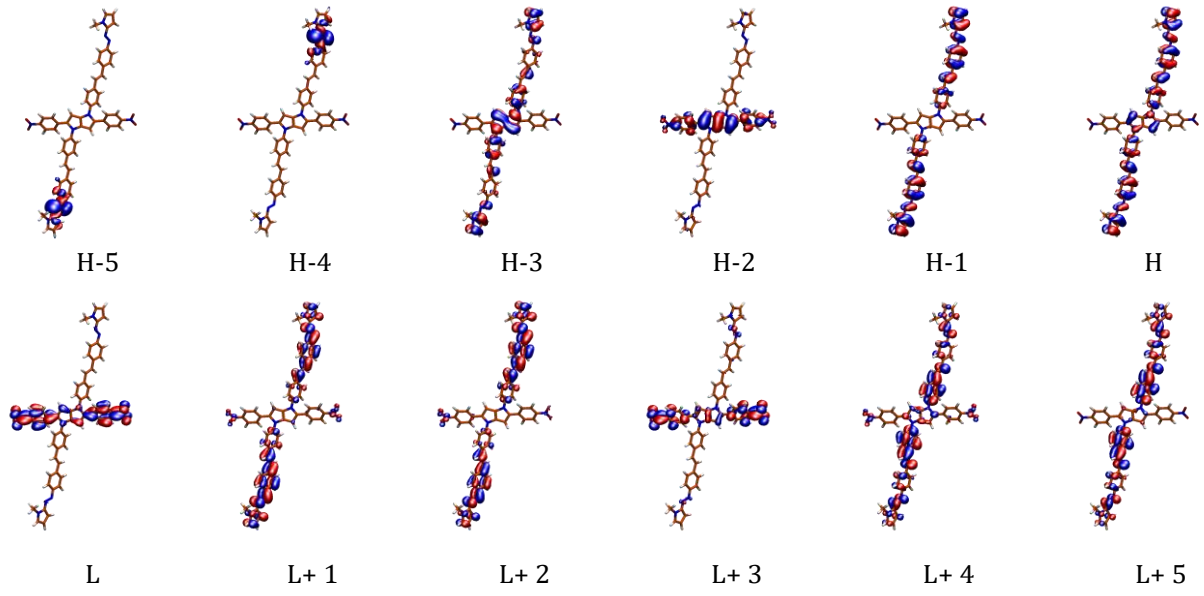

Figure S17. Iso-surface of the molecular orbitals involved in the description of the low energy singlet electronic states of **pp-4sap**.

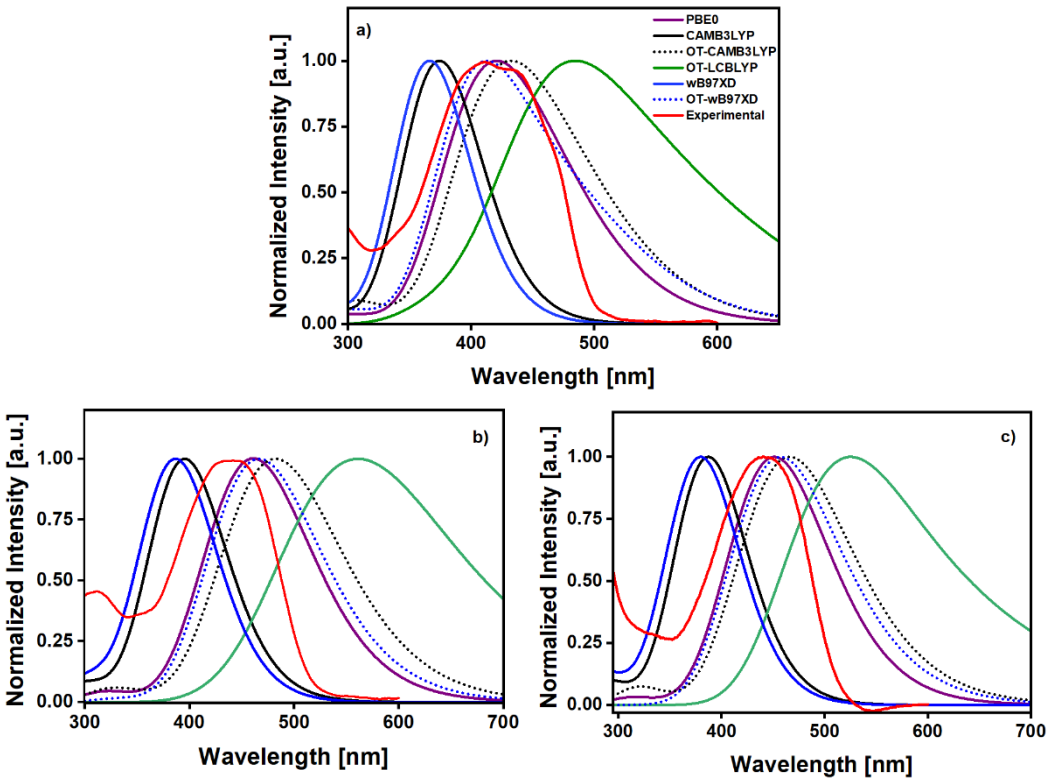

Figure S18. Simulated Electronic Absorption spectra for **pp-bap** (a), **pp-3sap** (b), and **pp-4sap** (c) using different density functional models, included the def2-SVP basis. The spectra were simulated from the calculated vertical transitions, and assuming a gaussian band shape with a width of 0.4 eV (standard deviation of the gaussian function).

Table S3. Excitation energies (eV), oscillator strengths *f*, electron transitions and their characters for **pp-bap** using TD-ωB97X-D/6-311+G//PCM=cyclohexane as level of theory. H=HOMO, L=LUMO. LE= localized excited state. bap= biphenyl azo pyrrole (actuator), pp= pyrrolopyrrole (antenna).

State	ΔE [eV]	*F*	Character	Nature	Transition
S_1	2.94	0.01	$^1n\pi^*$	LE (bap_1)	H-5→ L+2 (36) H-6→ L+2 (22) H-6→ L+3 (17)
S_2	2.94	0.01	$^1n\pi^*$	LE (bap_2)	H-5→ L+3 (40) H-6→ L+3 (17) H-6→ L+2 (15)
S_3	3.35	2.21	$^1\pi\pi^*$	LE (pp)	H→ L (77)
S_4	3.43	2.82	$^1\pi\pi^*$	LE ($bap_{1,2}$)	H-2→ L+3 (37) H-1→ L+2 (35)
S_5	3.45	0.00	$^1\pi\pi^*$	LE ($bap_{1,2}$)	H-2→ L+2 (42) H-1→ L+3 (39)
S_6	3.35	0.01	$^1\pi\pi^*$	LE (pp)	H→ L+1 (72)

Table S4. Excitation energies [eV], oscillator strengths *f*, electron transitions and their characters for **pp-4sap** using TD-ωB97X-D/6-311+G//PCM=cyclohexane as level of theory. H=HOMO, L=LUMO. LE= localized excited state, CT= charge transfer state, and ME= multiple excitations.

State	ΔE [eV]	*f*	Character	Nature	Transition
S_1	2.93	0.00	$^1n\pi^*$	LE (sap_2)	H-6→ L+2 (36) H-6→ L+1 (32)
S_2	2.94	0.04	$^1n\pi^*$	LE (sap_1)	H-7→ L+2 (28) H-7→ L+3 (17) H-7→ L+1 (16)
S_3	3.22	4.48	$^1\pi\pi^*$	LE/CT($sap_{1,2}$/pp→$sap_{1,2}$) LE/CT($sap_{1,2}$/$sap_{1,2}$→pp)	H→ L+2 (29) H-1→ L+1 (27)
S_4	3.26	0.14	$^1\pi\pi^*$	CT (sap→pp) ME (pp→sap)	H-1→ L+2 (39) H→ L+1 (20)
S_5	3.38	1.43	$^1\pi\pi^*$	LE (pp)	H-2→ L (65)
S_6	3.86	0.00	$^1\pi\pi^*$	LE (pp) CT (pp/sap→pp)	H-2→ L (37) H→ L (20)

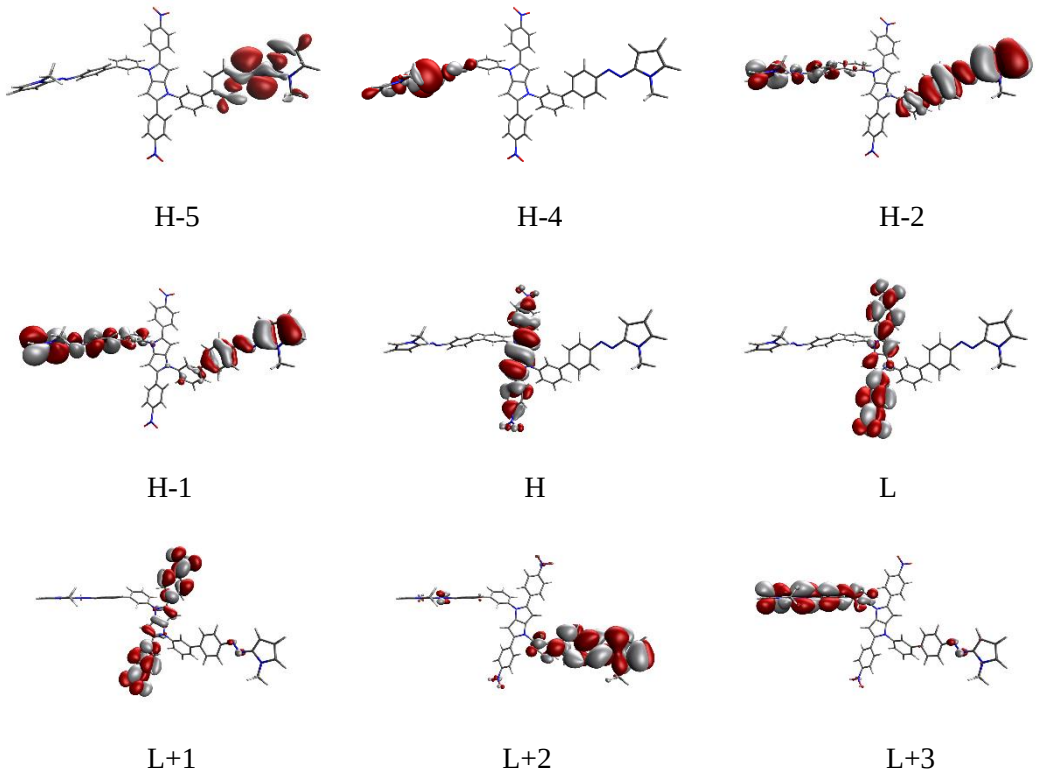

Figure S19. Iso-surface of the molecular orbitals involved in the description of the low energy singlet electronic states of **pp-3sap**.

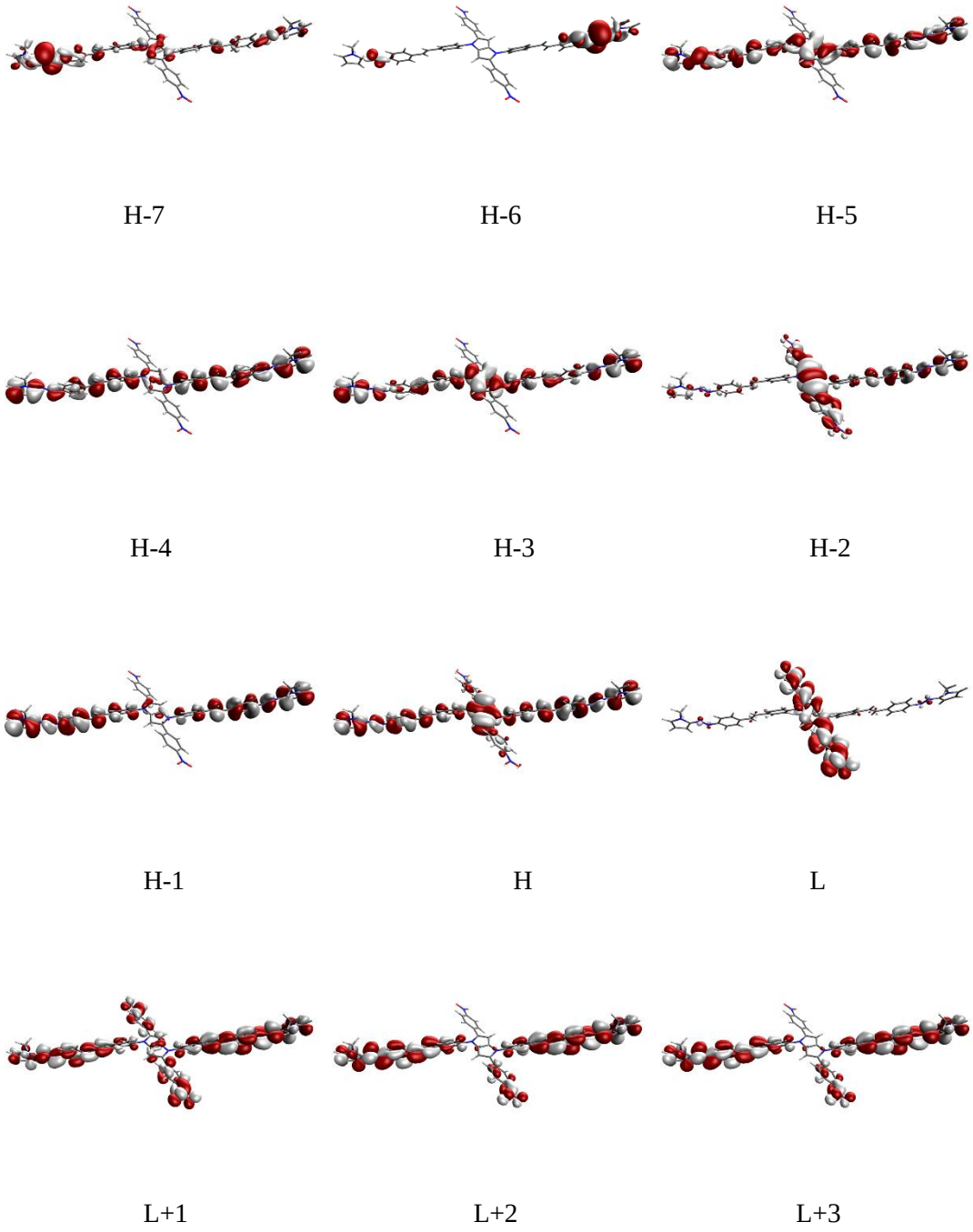

Figure S20. Iso-surface of the molecular orbitals involved in the description of the low energy singlet electronic states of **pp-4sap**.

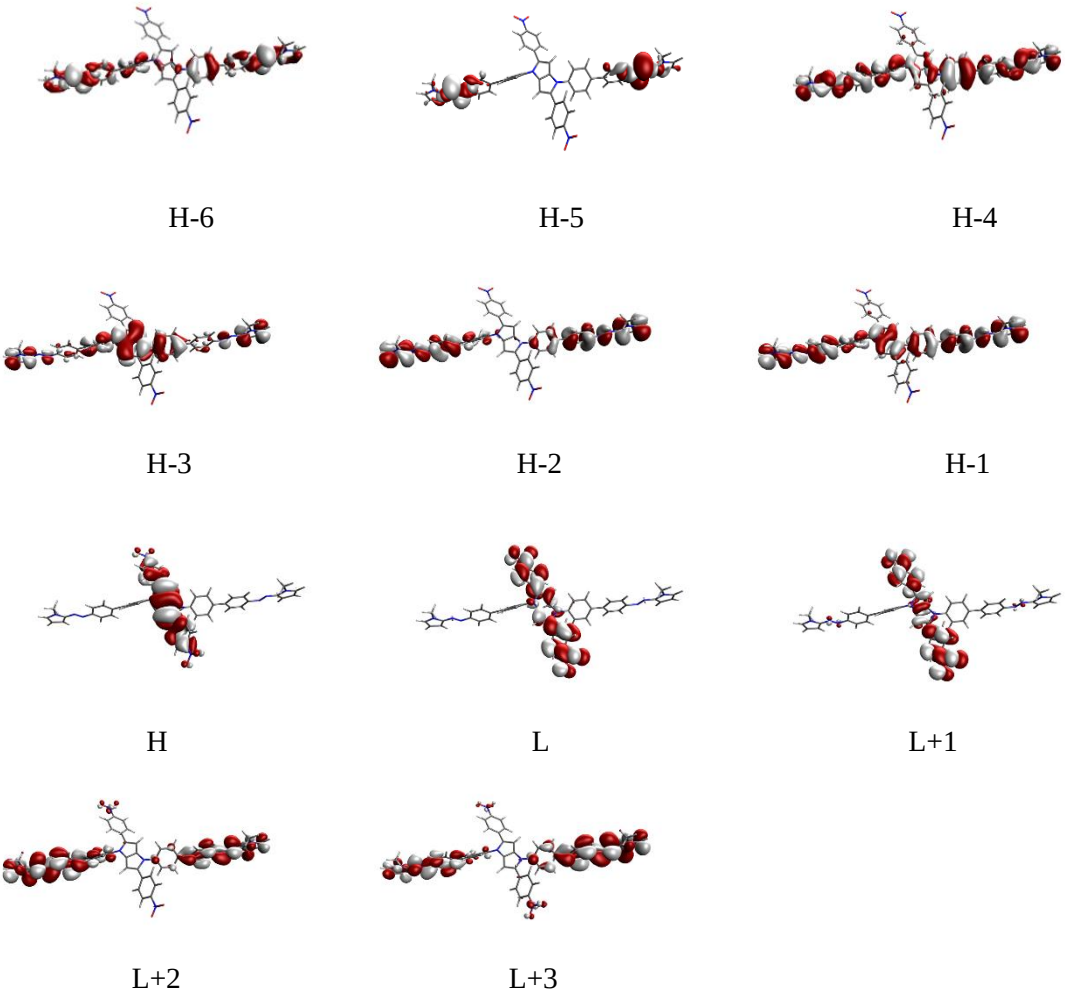

Figure S21. Iso-surface of the molecular orbitals involved in the description of the low energy singlet electronic states of **pp-bap**.

pp-pap Z-matrix (compact) coordinates ground state (OT-CAMB3LYP def2-SVP basis /PCM: cyclohexane)

0 1 (charge and multiplicity)
C
C 1 1.40059
C 2 1.41423 1 105.90637
N 1 1.40621 2 109.41887 3 358.81910
H 2 1.08653 1 125.16514 3 184.60608
C 3 2.28892 2 144.36447 1 7.04669
C 6 1.40059 3 70.52422 2 172.95852
N 3 1.38303 2 142.71305 1 175.66279
H 6 1.08653 3 163.99416 2 342.27423
C 4 1.38303 1 107.55058 2 0.26195
C 1 1.46162 2 126.43748 3 172.89797
C 11 1.41346 1 122.26087 2 217.63933
C 11 1.41306 1 119.33472 2 35.44274
C 12 1.39003 11 120.92930 1 178.33958
H 12 1.08972 11 120.01147 1 359.55220
C 13 1.38970 11 121.15800 1 181.94478
H 13 1.09122 11 119.34052 1 3.29102
C 14 1.39677 12 119.08472 11 359.65829
H 14 1.08924 12 121.55401 11 180.33826
H 16 1.08924 13 121.72875 11 180.46109
C 7 1.46162 6 126.43747 3 173.91884
C 21 1.41346 7 122.26084 6 217.63939
C 21 1.41306 7 119.33473 6 35.44269
C 22 1.39003 21 120.92931 7 178.33955
H 22 1.08972 21 120.01142 7 359.55216
C 23 1.38970 21 121.15798 7 181.94475
H 23 1.09122 21 119.34053 7 3.29112
C 24 1.39677 22 119.08472 21 359.65827
H 24 1.08924 22 121.55404 21 180.33819
H 26 1.08924 23 121.72875 21 180.46109
N 18 1.46723 14 119.22089 12 179.94067
O 31 1.22373 18 117.77657 14 179.68242
O 31 1.22362 18 117.79791 14 359.72211
N 28 1.46723 24 119.22092 22 179.94063
O 34 1.22373 28 117.77659 24 179.68175
O 34 1.22362 28 117.79788 24 359.72285
C 8 1.42068 3 123.53981 2 356.07184
C 37 1.40062 8 119.49422 3 55.01296
C 37 1.40113 8 120.95613 3 236.40020
C 38 1.39382 37 120.06421 8 181.11256
H 38 1.09177 37 119.54449 8 1.27268
C 39 1.39258 37 119.95987 8 179.71393
H 39 1.09088 37 119.75294 8 359.27995
C 40 1.40788 38 121.30401 37 359.35434
H 40 1.09159 38 119.00841 37 178.57442
H 42 1.09153 39 118.92644 37 178.20770

C 44 1.48202 40 121.15461 38 180.44556
C 47 1.40776 44 121.11150 40 213.43581
C 47 1.41221 44 120.96419 40 33.35753
C 48 1.39199 47 120.93816 44 179.79700
H 48 1.09191 47 119.71886 44 1.41487
C 49 1.38872 47 121.44882 44 180.06588
H 49 1.09239 47 119.38387 44 1.61916
C 50 1.40519 48 120.69732 47 0.15472
H 50 1.09170 48 121.30749 47 180.67471
H 52 1.09015 49 121.14238 47 180.61349
N 54 1.40581 50 116.21073 48 180.06686
C 57 2.23290 54 148.43937 50 180.70093
C 58 1.40450 57 103.39915 54 180.86799
N 58 1.38845 57 148.63291 54 1.18553
C 59 1.40655 58 107.01449 57 180.17607
H 59 1.08655 58 124.40945 57 0.22373
C 60 1.35958 58 108.72773 57 179.65741
H 61 1.08809 59 127.23894 58 180.00789
H 63 1.08816 60 120.80767 58 180.03098
N 57 1.26553 54 115.10477 50 180.98584
C 60 1.45230 58 125.01287 57 359.68343
H 67 1.09928 60 110.70068 58 299.57852
H 67 1.09918 60 110.68012 58 59.65138
H 67 1.09750 60 108.66689 58 179.61131
C 4 1.42068 1 127.90030 2 191.56683
C 71 1.40062 4 119.49426 1 222.05471
C 71 1.40113 4 120.95613 1 43.44196
C 72 1.39382 71 120.06423 4 181.11252
H 72 1.09177 71 119.54442 4 1.27272
C 73 1.39258 71 119.95993 4 179.71394
H 73 1.09088 71 119.75289 4 359.27996
C 74 1.40788 72 121.30400 71 359.35440
H 74 1.09159 72 119.00842 71 178.57439
H 76 1.09153 73 118.92646 71 178.20766
C 78 1.48202 74 121.15460 72 180.44557
C 81 1.40776 78 121.11147 74 213.43574
C 81 1.41221 78 120.96417 74 33.35744
C 82 1.39199 81 120.93808 78 179.79700
H 82 1.09191 81 119.71893 78 1.41487
C 83 1.38872 81 121.44880 78 180.06594
H 83 1.09239 81 119.38385 78 1.61917
C 84 1.40519 82 120.69734 81 0.15469
H 84 1.09170 82 121.30741 81 180.67472
H 86 1.09015 83 121.14238 81 180.61356
C 88 3.50878 84 135.66460 82 179.73264
C 91 1.40450 88 115.50259 84 1.83500
N 91 1.38845 88 136.52987 84 181.79678
C 92 1.40655 91 107.01446 88 179.97465
H 92 1.08655 91 124.40948 88 0.02225
C 93 1.35958 91 108.72766 88 180.01846

H 94 1.08809 92 127.23886 91 180.00784
H 96 1.08816 93 120.80768 91 180.03095
N 88 1.40581 84 116.21068 82 180.06692
N 99 1.26553 88 115.10468 84 180.98575
C 93 1.45230 91 125.01293 88 0.04440
H 101 1.09928 93 110.70070 91 299.57858
H 101 1.09918 93 110.68009 91 59.65136
H 101 1.09750 93 108.66687 91 179.61133

pp-3sap Z-matrix (compact) coordinates ground state (OT-CAMB3LYP def2-SVP basis /PCM: toluene)

0 1 (charge and multiplicity)
C
C 1 1.39733
C 2 1.41733 1 105.85709
C 3 1.40116 2 108.79680 1 358.05180
N 4 1.38446 3 108.29862 2 1.74658
N 3 1.38446 2 142.66066 1 184.85012
C 6 1.40867 3 107.40178 2 172.39330
C 7 1.39733 6 109.60920 3 359.59467
C 7 1.46581 6 123.08111 3 176.25889
C 9 1.41120 7 119.66237 6 138.42370
C 10 1.39199 9 120.96505 7 184.06220
C 11 1.39726 10 118.84595 9 359.05366
C 12 1.39813 11 121.70033 10 358.42063
C 13 1.39015 12 118.89288 11 2.21130
C 1 1.46581 2 127.21323 3 184.95296
C 15 1.41119 1 119.66234 2 314.47641
C 16 1.39199 15 120.96509 1 184.06210
C 17 1.39726 16 118.84590 15 359.05384
C 18 1.39813 17 121.70038 16 358.42064
C 19 1.39015 18 118.89284 17 2.21119
C 5 1.42064 4 124.79629 3 189.81824
C 21 1.39680 5 119.90603 4 133.46565
C 22 1.40660 21 121.09040 5 175.24634
C 23 1.40982 22 118.12957 21 5.90316
C 24 1.39645 23 120.56140 22 356.90529
C 25 1.39776 24 120.76153 23 358.91219
C 6 1.42065 3 124.79556 2 3.04361
C 27 1.39680 6 119.90634 3 133.46090
C 28 1.40660 27 121.09041 6 175.24763
C 29 1.40981 28 118.12959 27 5.90245
C 30 1.39645 29 120.56146 28 356.90582
C 31 1.39776 30 120.76150 29 358.91215

C 23 1.46641 22 121.36422 21 188.29672
C 33 1.35402 23 124.41882 22 20.39096
C 34 1.46067 33 127.57986 23 177.10440
C 35 1.41102 34 118.85713 33 189.06047
C 36 1.39137 35 121.15242 34 178.58487
C 37 1.40609 36 120.51855 35 0.47809
C 38 1.41430 37 118.88365 36 0.00498
C 39 1.38573 38 120.30739 37 359.76909
N 38 1.40334 37 116.26777 36 179.89438
N 41 1.26759 38 115.26796 37 179.89964
C 42 1.36588 41 115.99664 38 180.07682
C 43 1.40545 42 134.01032 41 0.07153
N 43 1.38940 42 118.05843 41 180.02465
C 45 1.36026 43 108.73758 42 180.01912
C 46 1.39820 45 108.97333 43 0.01039
C 45 1.45328 43 125.03347 42 0.01469
C 29 1.46641 28 121.36410 27 188.29513
C 49 1.35402 29 124.41894 28 20.39125
C 50 1.46067 49 127.57987 29 177.10598
C 51 1.41101 50 118.85719 49 189.05967
C 52 1.39137 51 121.15243 50 178.58579
C 53 1.40609 52 120.51854 51 0.47834
C 54 1.41430 53 118.88361 52 0.00432
C 55 1.38573 54 120.30746 53 359.76969
N 54 1.40334 53 116.26784 52 179.89356
N 57 1.26759 54 115.26803 53 179.90080
C 58 1.36588 57 115.99646 54 180.07593
C 59 1.40545 58 134.01027 57 0.07084
C 60 1.40687 59 107.03306 58 179.97246
C 61 1.39820 60 107.32478 59 359.99054
N 62 1.36026 61 108.97342 60 359.99978
C 63 1.45328 62 126.22901 61 180.01530
N 12 1.46741 11 119.15146 10 177.52560
O 65 1.22666 12 117.64487 11 348.48545
O 65 1.22248 12 117.94006 11 168.95376
N 18 1.46741 17 119.15145 16 177.52545
O 68 1.22666 18 117.64498 17 348.48666
O 68 1.22248 18 117.93997 17 168.95311
H 2 1.08645 1 124.94337 3 175.97411
H 8 1.08646 7 124.94349 6 177.41684
H 10 1.09134 9 119.33526 7 1.05954
H 11 1.08917 10 121.56017 9 177.75022
H 13 1.08907 12 119.47839 11 181.43002
H 14 1.09025 13 119.31700 12 179.30170
H 16 1.09134 15 119.33524 1 1.05943
H 17 1.08917 16 121.56019 15 177.75028
H 19 1.08907 18 119.47841 17 181.42976
H 20 1.09025 19 119.31699 18 179.30148
H 22 1.08797 21 119.27709 5 355.70100
H 24 1.09258 23 119.42816 22 178.47669

H 25 1.09223 24 119.79563 23 180.73198
H 26 1.09098 25 120.81012 24 183.27633
H 28 1.08797 27 119.27716 6 355.70130
H 30 1.09258 29 119.42824 28 178.47659
H 31 1.09223 30 119.79571 29 180.73164
H 32 1.09098 31 120.81003 30 183.27586
H 33 1.09449 23 115.73038 22 196.06570
H 34 1.09476 33 118.17323 23 0.02833
H 36 1.09253 35 119.61573 34 359.22448
H 37 1.09144 36 121.15851 35 180.74678
H 39 1.09004 38 118.60064 37 179.62266
H 40 1.09222 39 119.04872 38 179.54565
H 44 1.08650 43 124.41626 42 0.02672
H 46 1.08805 45 120.81690 43 179.98366
H 47 1.08807 46 125.44377 45 179.96215
H 48 1.09921 45 110.70725 43 60.42637
H 48 1.09910 45 110.66675 43 300.34464
H 48 1.09737 45 108.67296 43 180.39893
H 49 1.09449 29 115.73034 28 196.06697
H 50 1.09476 49 118.17318 29 0.02913
H 52 1.09253 51 119.61590 50 359.22506
H 53 1.09144 52 121.15860 51 180.74644
H 55 1.09004 54 118.60055 53 179.62302
H 56 1.09222 55 119.04876 54 179.54527
H 60 1.08650 59 124.41634 58 0.02698
H 61 1.08807 60 127.23137 59 180.02878
H 62 1.08805 61 130.20981 60 180.02961
H 64 1.09737 63 108.67285 62 0.38937
H 64 1.09921 63 110.70716 62 240.41693
H 64 1.09910 63 110.66691 62 120.33503

pp-4sap Z-matrix (compact) coordinates ground state (OT-CAMB3LYP def2-SVP basis /PCM: toluene)

0 1 (charge and multiplicity)
C
C 1 1.40164
C 2 1.41389 1 105.95737
N 1 1.40767 2 109.38426 3 0.02867
H 2 1.08641 1 125.16775 3 176.12108
C 3 2.28947 2 144.60081 1 0.33882
C 6 1.40167 3 70.55445 2 179.64606
N 3 1.38402 2 142.85311 1 179.38085
H 6 1.08642 3 163.87186 2 347.52925
C 4 1.38402 1 107.51751 2 359.60521
C 1 1.46180 2 126.39571 3 185.26697
C 11 1.41450 1 122.30417 2 142.74207

C 11 1.41408 1 119.37547 2 325.14874
C 12 1.39027 11 120.97369 1 181.76664
H 12 1.08943 11 120.03975 1 0.46363
C 13 1.38997 11 121.20679 1 177.94328
H 13 1.09099 11 119.36804 1 356.56796
C 14 1.39779 12 119.12602 11 0.36147
H 14 1.08904 12 121.43747 11 179.65126
H 16 1.08902 13 121.63471 11 179.50109
C 7 1.46183 6 126.40473 3 174.49597
C 21 1.41447 7 122.29140 6 217.22155
C 21 1.41407 7 119.38352 6 34.81955
C 22 1.39031 21 120.97236 7 178.22453
H 22 1.08945 21 120.03930 7 359.52920
C 23 1.38997 21 121.20228 7 182.07056
H 23 1.09099 21 119.37373 7 3.43864
C 24 1.39774 22 119.12281 21 359.63127
H 24 1.08904 22 121.44170 21 180.34330
H 26 1.08902 23 121.63382 21 180.49048
N 18 1.46720 14 119.27351 12 180.17449
O 31 1.22494 18 117.83892 14 180.72651
O 31 1.22476 18 117.86385 14 0.72856
N 28 1.46732 24 119.26903 22 179.86728
O 34 1.22488 28 117.83455 24 179.33265
O 34 1.22472 28 117.85882 24 359.34519
C 8 1.42144 3 123.64386 2 350.14466
C 37 1.40063 8 119.61173 3 55.14484
C 37 1.40461 8 120.88346 3 236.60813
C 38 1.39397 37 119.91013 8 181.09476
H 38 1.09148 37 119.62886 8 1.86711
C 39 1.39005 37 120.18432 8 179.70277
H 39 1.09079 37 119.62012 8 359.95490
C 40 1.41050 38 121.60290 37 359.29176
H 40 1.09274 38 119.26613 37 180.13776
H 42 1.09115 39 118.57991 37 179.96045
C 44 1.46352 40 119.03074 38 180.74091
C 47 1.35351 44 126.72653 40 178.00789
H 47 1.09433 44 114.42559 40 358.28041
H 48 1.09470 47 118.73675 44 359.73009
C 48 1.46106 47 126.92250 44 179.97284
C 51 1.41118 48 118.97201 47 178.95579
C 51 1.41756 48 123.38617 47 358.98108
C 52 1.39147 51 121.27563 48 180.12217
H 52 1.09302 51 119.06334 48 0.04111
C 53 1.38547 51 121.39707 48 179.88761
H 53 1.09192 51 119.75599 48 359.82253
C 54 1.40630 52 120.54517 51 359.95790
H 54 1.09164 52 121.40596 51 179.92816
H 56 1.09000 53 121.04041 51 180.00034
N 58 1.40279 54 116.27104 52 179.95120
C 61 2.23440 58 148.60907 54 180.12408

C 62 1.40588 61 103.36591 58 179.44736
N 62 1.38973 61 148.72416 58 359.29290
C 63 1.40673 62 107.04385 61 179.86881
H 63 1.08649 62 124.45701 61 359.77676
C 64 1.36022 62 108.74163 61 180.22744
H 65 1.08806 63 127.23719 62 179.94483
H 67 1.08803 64 120.82126 62 179.93605
N 61 1.26812 58 115.29352 54 179.94076
C 64 1.45360 62 125.03454 61 359.87636
H 71 1.09936 64 110.74969 62 298.12422
H 71 1.09885 64 110.59953 62 58.20964
H 71 1.09734 64 108.68470 62 178.14088
C 4 1.42149 1 127.89034 2 168.79625
C 75 1.40100 4 121.02294 1 315.67171
C 75 1.40409 4 119.46896 1 136.82603
C 76 1.39277 75 119.80763 4 179.98850
H 76 1.09073 75 119.81338 4 359.92274
C 77 1.39128 75 120.28015 4 179.22056
H 77 1.09158 75 119.43380 4 358.38871
C 78 1.41120 76 121.72766 75 1.03584
H 78 1.09269 76 119.18859 75 180.34720
H 80 1.09121 77 118.66682 75 179.81670
C 82 1.46360 78 118.99062 76 179.89606
C 85 1.35350 82 126.74946 78 180.05906
H 85 1.09429 82 114.40198 78 0.13684
H 86 1.09476 85 118.73600 82 0.16233
C 86 1.46106 85 126.92926 82 180.18618
C 89 1.41119 86 118.98682 85 180.40365
C 89 1.41755 86 123.37781 85 0.44473
C 90 1.39149 89 121.28163 86 180.01129
H 90 1.09304 89 119.06793 86 0.01510
C 91 1.38545 89 121.39703 86 179.98286
H 91 1.09190 89 119.75748 86 0.06185
C 92 1.40625 90 120.54546 89 0.01555
H 92 1.09161 90 121.40364 89 179.98935
H 94 1.09000 91 121.02737 89 180.04417
C 96 3.50874 92 135.72241 90 179.89709
C 99 1.40588 96 115.45892 92 359.90859
N 99 1.38981 96 136.62959 92 179.98036
C 100 1.40667 99 107.04361 96 180.04508
H 100 1.08647 99 124.46206 96 0.01434
C 101 1.36017 99 108.73685 96 179.93840
H 102 1.08805 100 127.24027 99 179.99380
H 104 1.08806 101 120.84916 99 180.01075
N 96 1.40294 92 116.29250 90 179.94420
N 107 1.26813 96 115.23590 92 180.01712
C 101 1.45374 99 125.02047 96 359.95219
H 109 1.09910 101 110.68062 99 299.95350
H 109 1.09910 101 110.67298 99 60.04638
H 109 1.09730 101 108.69437 99 179.99923

Time Correlated Single Photon Counting (TCSPC) Measurements

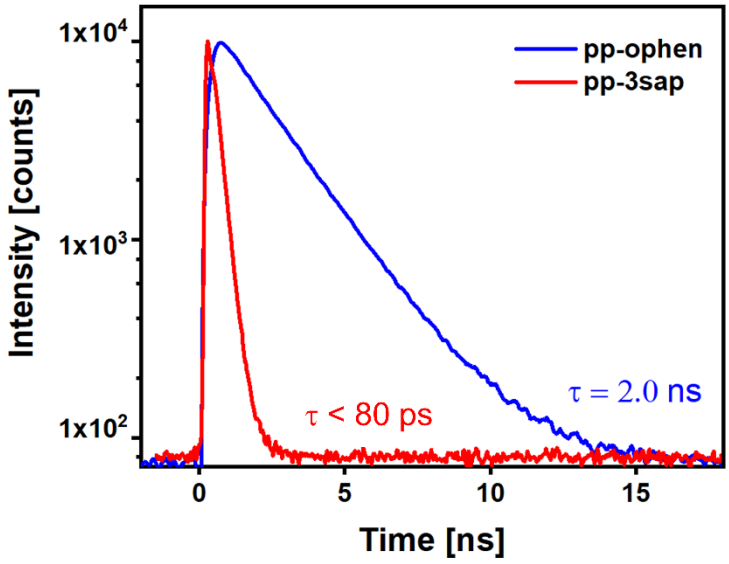

Figure S22. TCSPC traces of **pp-ophen** (blue line) and **pp-3sap** (red line) in toluene solution at room temperature.

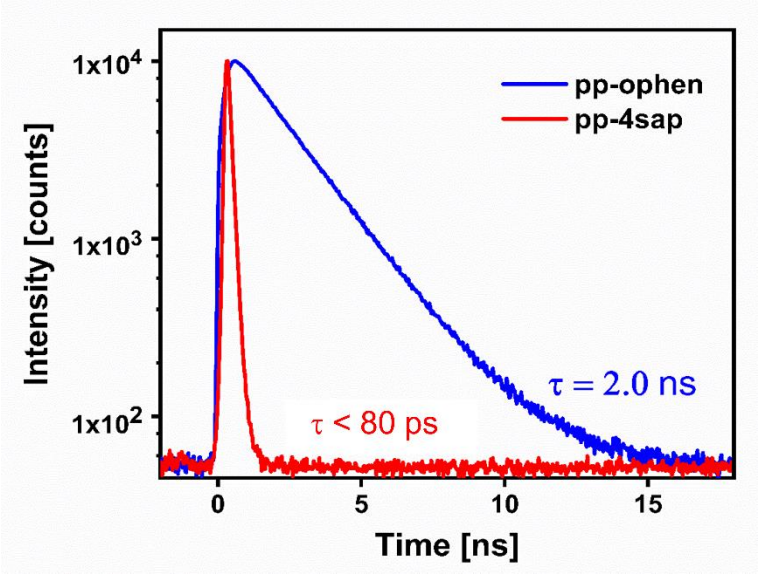

Figure S23. TCSPC traces of **pp-ophen** (blue line) and **pp-4sap** (red line) in toluene solution at room temperature.

Linear Photochemical Transformations

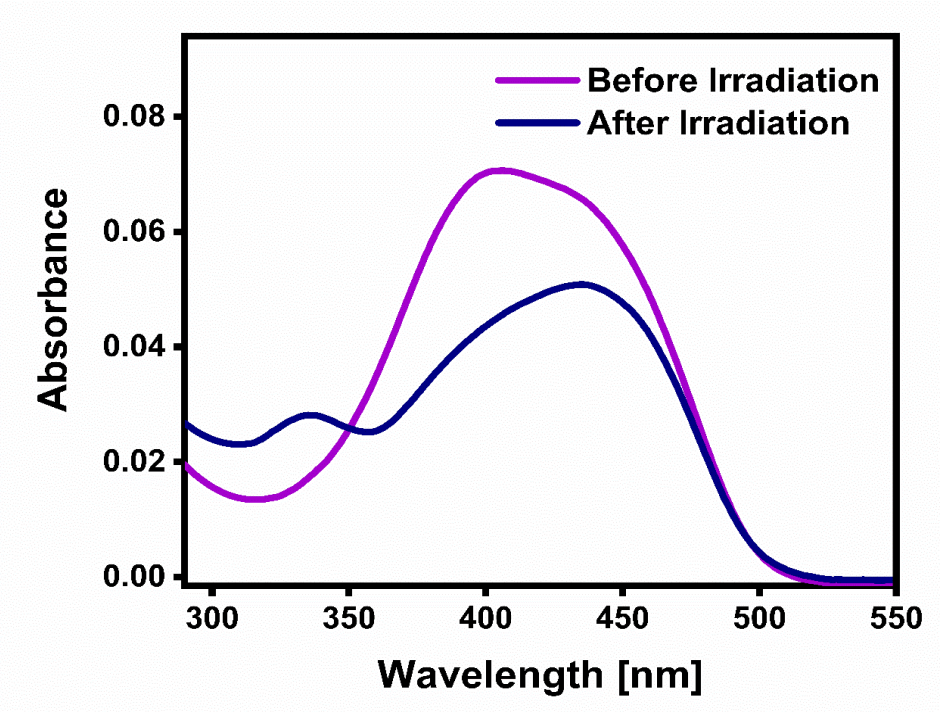

Figure S24. Absorption Spectra of **pp-bap** and its single-photon transformation upon 400 nm excitation in cyclohexane solution.

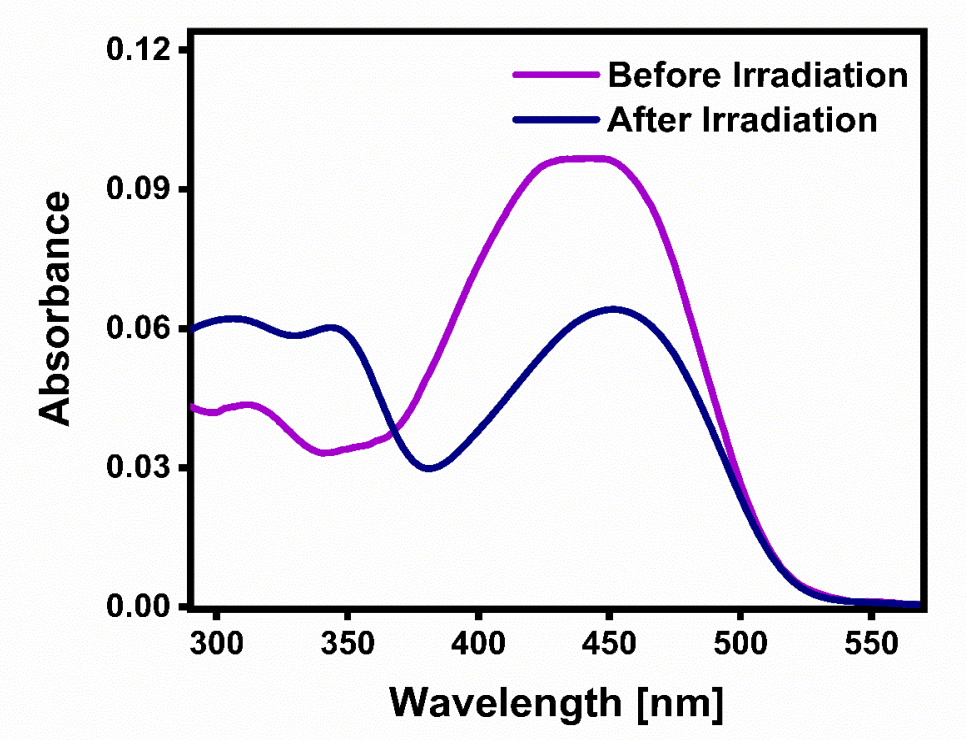

Figure S25. Absorption Spectra of **pp-3sap** and its single-photon transformation upon 400 nm excitation in toluene solution.

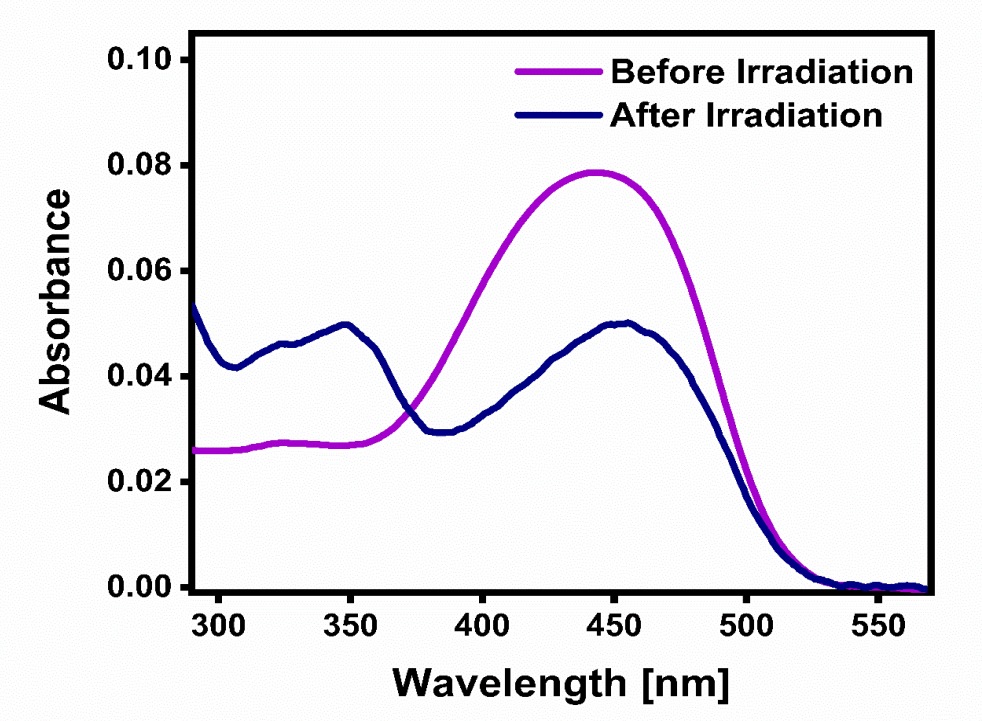

Figure S26. Absorption Spectra of **pp-4sap** and its single-photon transformation upon 400 nm excitation in toluene solution.

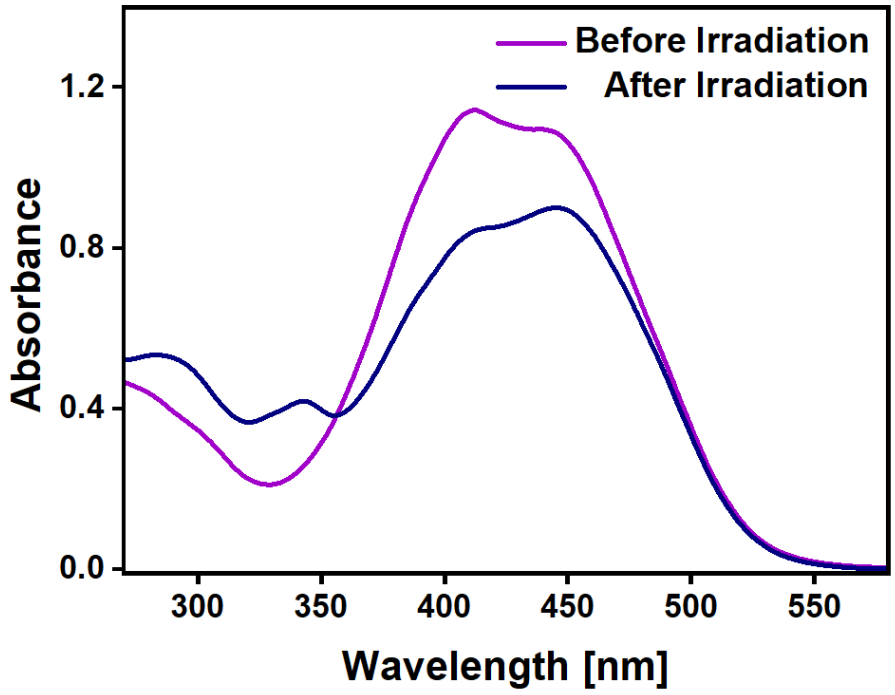

Figure S27. Absorption Spectra of **pp-bap** and its single-photon transformation upon 450 nm excitation in a cyclohexane-chloroform 55:45 mixture solution.

Thermal-back equilibration after monophotonic excitation

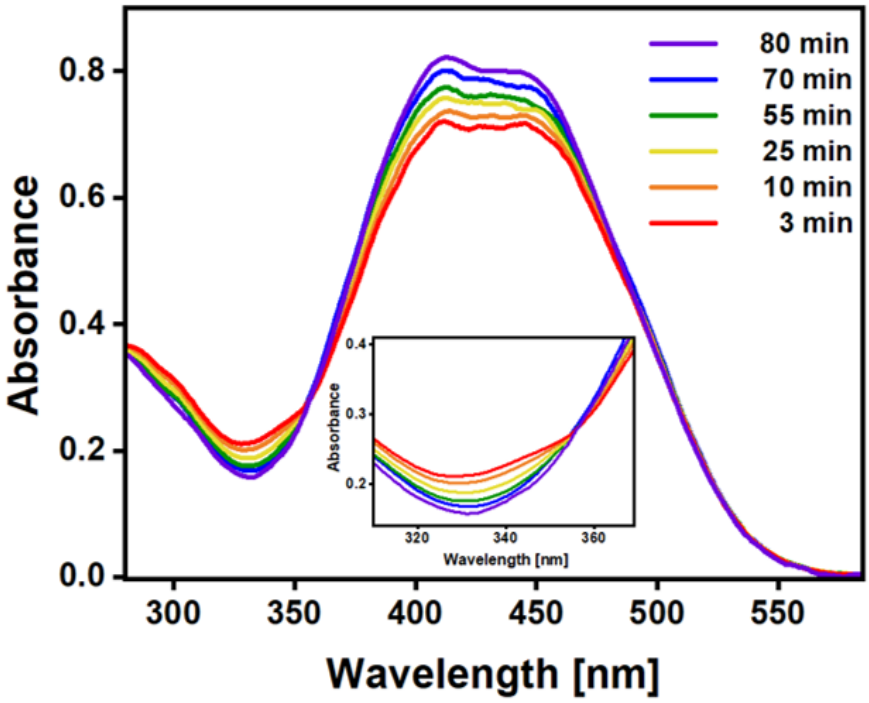

Figure S28. Absorption spectra of **pp-bap** in $CDCl_3$ solution at 21 °C showing the thermal back-isomerization kinetics after 450 nm irradiation. The purple line is the spectrum after 80 minutes of the irradiation and corresponds the initial spectrum. Inset: shows the isosbestic point localized at 357 nm.

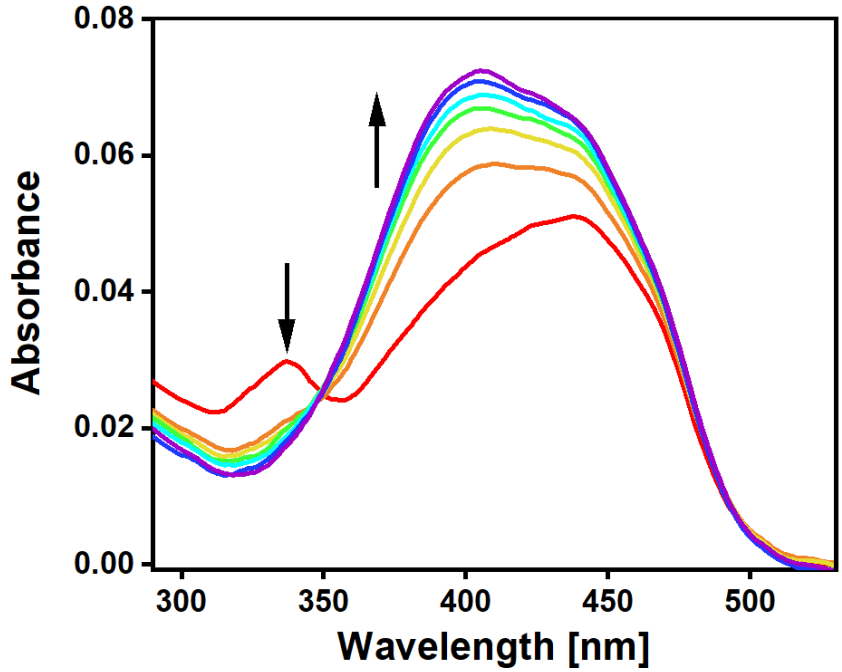

Figure S29. Absorption spectra showing the back thermal of **pp-bap** from *Z*-isomer to *E*-isomer after monophotonic excitation in cyclohexane solution.

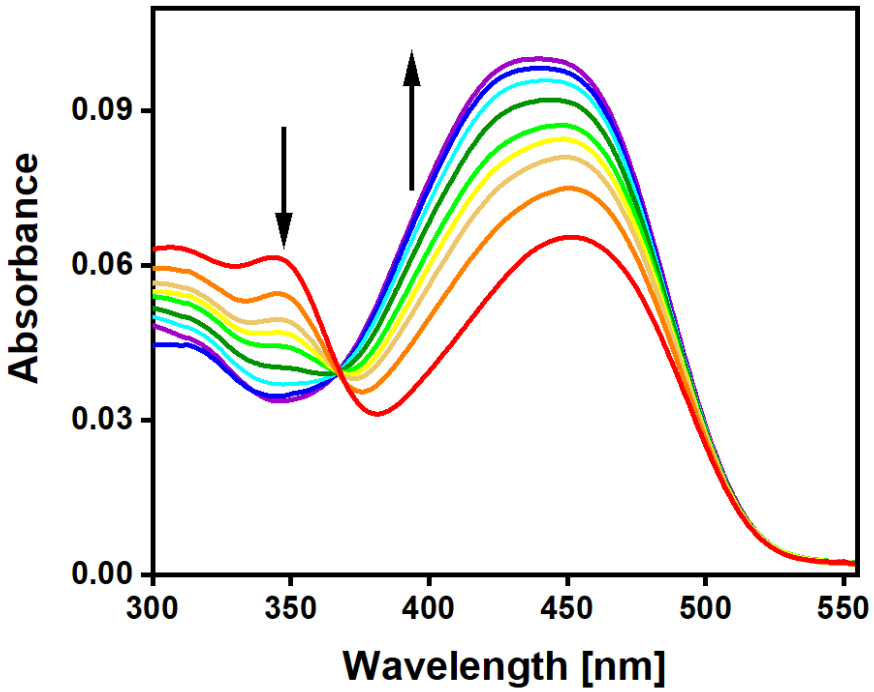

Figure S30. Absorption Spectra showing the thermal equilibration of **pp-3sap** after monophotonic excitation in toluene solution.

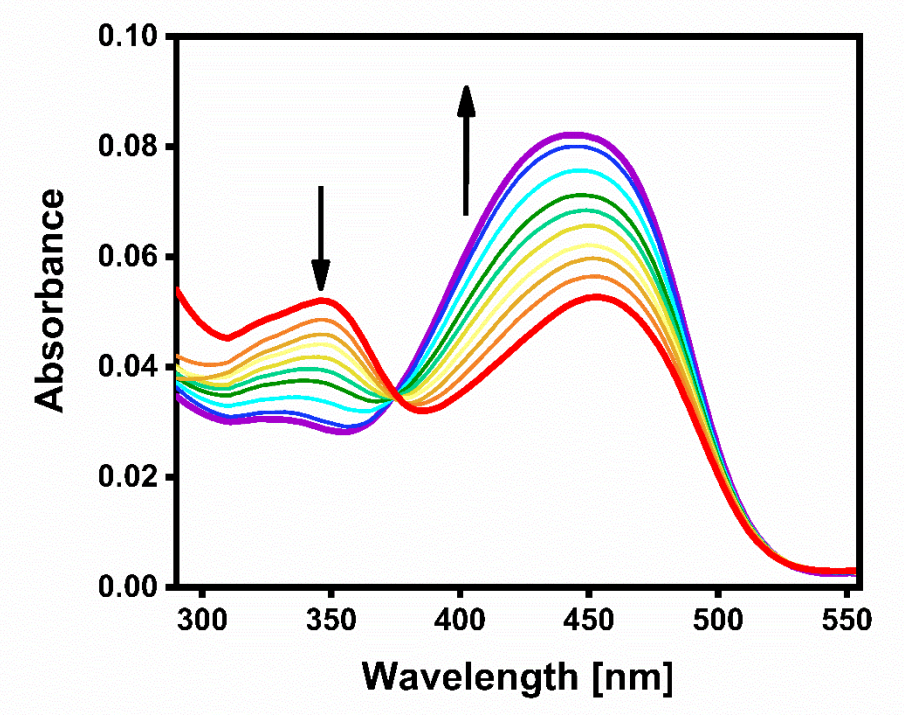

Figure S31. Absorption Spectra showing the thermal equilibration of **pp-4sap** after monophotonic excitation in toluene solution.

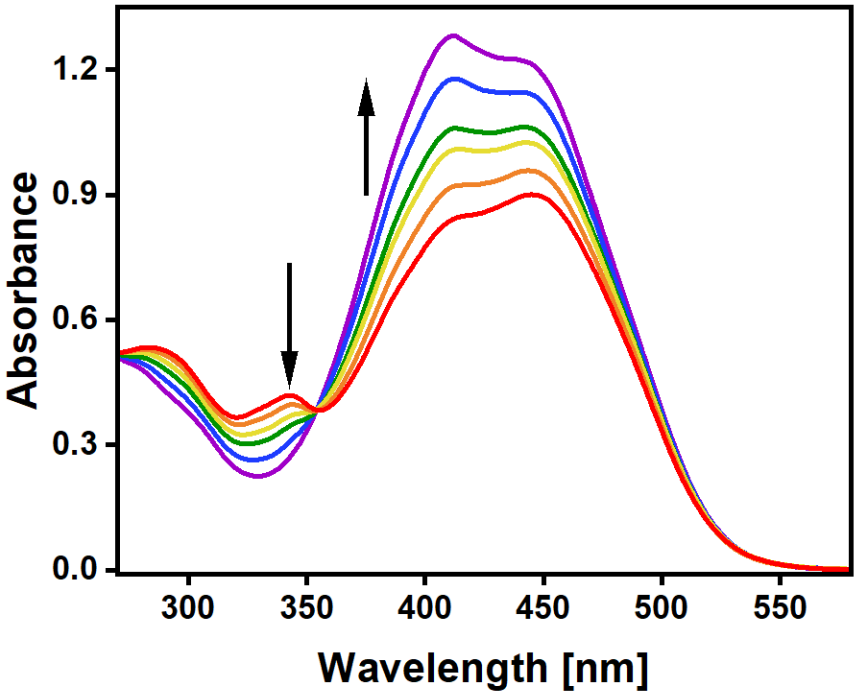

Figure S32. Absorption Spectra showing the thermal equilibration of **pp-bap** after monophotonic excitation in a cyclohexane-chloroform 55:45 mixture.

Kinetics of the thermal return to the original isomer form of pp-bap, pp-3sap and pp-4bap

Table S5. Amplitudes and lifetime values obtained by Levenberg-Marquadt non-linear fits on the thermal return kinetics of **pp-bap**, **pp-3sap**, and **pp-4sap** after monophotonic(400 nm) and biphotonic (800 nm) excitation shown in Figure S33. These kinetics models correspond to following biexponential function: $|Abs|(t)=\alpha_1 \exp(-t/\tau_1) +\alpha_2 \exp(-t/\tau_2)$. The time constants were obtained by a global fitting procedure taking both the 400 nm excitation and the 800 nm excitation traces together for each molecule to produce simultaneously-adjusted time-constants. The experimental traces and the fitting curves are shown in Figure S33.

	1PA				**2PA**			
Molecule	α_1	τ_1 [min]	α_2	τ_2 [min]	α_1	τ_1 [min]	α_2	τ_2 [min]
pp-bap	0.015	24	0.012	1.4	0.013	24	0.0002	1.4
pp-3sap	0.071	18	0.016	1	0.012	18	0.006	1
pp-4sap	0.003	28	0.0004	3.3	0.085	28	0.056	3.3

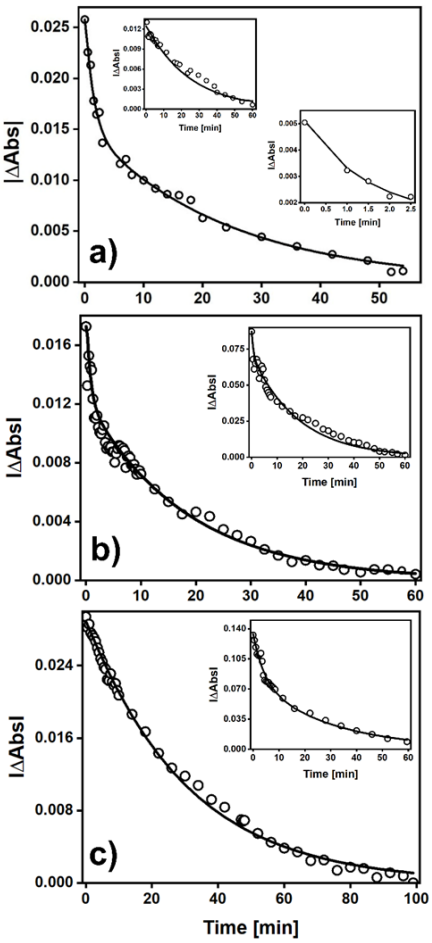

Figure S33. Evolution of the change in the absorbance of a) cyclohexane solutions of **pp-bap**, b) toluene solutions of **pp-3sap**, and c) toluene solutions of **pp-4sap** from photo-converted states back to the thermally equilibrated states after monophotonic 400 nm excitation (main graphs) and biphotonic 800 nm excitation (insets). The traces show the absolute values of the absorbance changes with respect to the pre-irradiated solutions as a function of time. The changes on the absorbances were measured at 413, 438 and 440 nm for **pp-bap**, **pp-3sap** and **pp-4sap** respectively. The t=0 value in these graphs correspond to the moment when the irradiation on the solution was stopped to allow for the thermal returns. The solid lines show non-linear fits using the Levenberg-Marquardt algorithm, where the linear and biphotonic excitation traces were fitted together to obtain globally fitted decay time constants. The optimal parameters for the biexponential decay curves are included in Table S5.

For biphotonic excitation it is more difficult to see the biexponential form of the return to the original absorption spectrum since the fast-returning species (*E,Z* isomer), has a short lifetime, and biphotonic excitation, being a process with small probability, accumulates this species more slowly. This implies that both the rapid return to the *E,E* isomer and the progress (with an additional excitation) to the *Z,Z* isomer can make the *E,Z* species to be present in a small concentration (in a kinetic steady-state during biphotonic excitation). From this, in particular for molecule **pp-bap**, the biexponential behavior for biphotonic excitation was not as clear as for the other molecules. Therefore, we include in the graph insets a situation with short irradiation time to show the return of the fast-returning species (*E,Z*), and another one, with longer irradiation times where the long decay time is more dominant.

Estimation of the Absorption Spectra of the *Z*-isomers

For the estimation of the absorption spectra of *Z*-**bap** isomers from the photostationary spectra we used the method proposed by Calbo and collaborators.[3] From the Lambert-Beer law:

$$\mathrm{Abs_T}(\lambda) = \mathrm{Abs_E}(\lambda) + \mathrm{Abs_Z}(\lambda) \quad \text{(S1)}$$

where $\mathrm{Abs_T}(\lambda)$ is the total absorbance for the photo-stationary state as a function of the wavelength of the sample. Previous to the irradiation, the *E*-isomer of actuator-only **bap** is the only species present, so, Eq. S1 reduces to Eq. S2.

$$\mathrm{Abs_T}(\lambda) = \mathrm{Abs_E}(\lambda) = \varepsilon_E(\lambda) l C_0 \quad \text{(S2)}$$

where $\varepsilon_E(\lambda)$ is the absorptivity coefficient of *E*-isomer (in units of $M^{-1}cm^{-1}$) as a function of wavelength, l is the path length (in cm) and C_0 is the initial concentration (in mol/L) from a stock solution of actuator-only **bap** in cyclohexane solution with molar concentration known. The solution of *E*-**bap** irradiated with a light source undergoes a change of its geometry and a fraction is photo-isomerized to *Z*-isomer. It is known that the total concentration C_0 remains constant during the isomerization process. So that:

$$C_0 = C_E + C_z \quad \text{(S3)}$$

Combining Eq. S1 and Eq. S3, we have:

$$\mathrm{Abs_T}(\lambda) = \mathrm{Abs_E}(\lambda) + \mathrm{Abs_Z}(\lambda) = \varepsilon_E(\lambda) l C_E + \varepsilon_z(\lambda)\, l\, C_z \quad \text{(S4)}$$

Dividing Eq. S4 by lC_0 and rearranging, we obtain Eq. S5:

$$\frac{Abs_T(\lambda)}{lC_0} = \varepsilon_E f_E + \varepsilon_z(1 - f_E) \quad \text{(S5)}$$

where f_E represents the mole fraction of the *E*-isomer that remained after irradiation. From this equation, we estimated the absorptivity coefficient as function of wavelength for the *Z*-isomer.

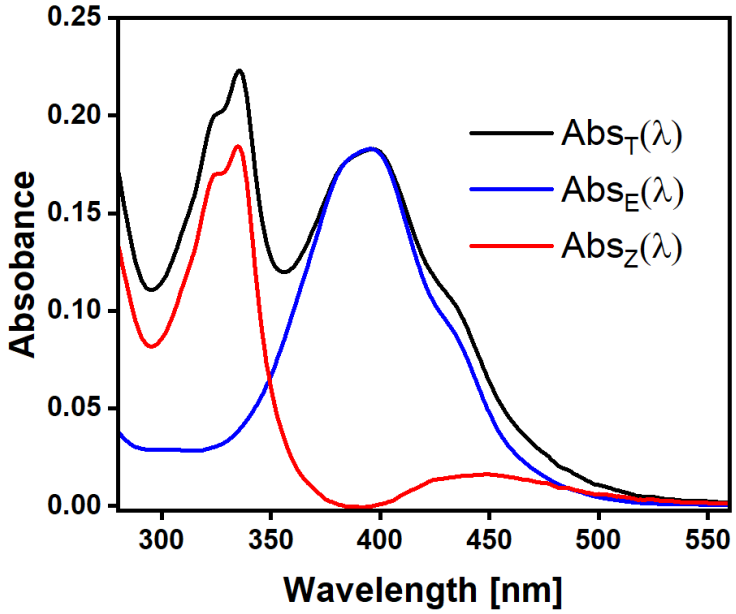

Figure S34. Absorption spectra of *E*-**bap** (blue line) and *Z*-**bap** (red line) in cyclohexane solution at room temperature using the Calbo Method. $Abs_T(\lambda)$ (black line) is the experimental spectrum after irradiation at 450 nm for only ten seconds, and correspond to the photoconverted mixture where a fraction of the total **bap** molecules have been converted to the *Z* isomer. The photo-isomerized mole fraction for the *Z*-isomer of actuator-only **bap** was 0.62.

Reconstruction of spectra of photo-converted samples based on the spectra of the individual units

From the analysis of the absorption coefficients of actuator-only **bap**, analogously we reconstructed the experimental spectrum of **pp-bap** after irradiation at 450 nm in cyclohexane solution. The spectrum was re-constructed as the algebraic sum of its components as following Eq. S6.

$$Abs_{\mathbf{pp-bap}}^{irradiated} = C_{\mathbf{pp-bap}}\{\varepsilon_{\mathbf{pp-ophen}} + f_E 2\varepsilon(\lambda)_E + (1 - f_E)2\varepsilon(\lambda)_Z\} \qquad (S6)$$

Where $C_{\mathbf{pp\text{-}bap}}$ is the known molar concentration [mol/L] of **pp-bap** in cyclohexane solution, $\varepsilon_{\mathbf{pp\text{-}ophen}}$ represents the molar absorptivity [$M^{-1}cm^{-1}$] for **pp-ophen** in cyclohexane solution shown in Figure 5a, f_E corresponds to the molar fraction of the *E*-isomer actuator-only **bap** and (1- f_E) corresponds to the molar fraction of the *Z*-isomer actuator-only **bap**. $\varepsilon(\lambda)_E$ and $\varepsilon(\lambda)_Z$ are the molar absorptivities as functions of the wavelength obtained for *E*-**bap** and *Z*-**bap** respectively using the Calbo Method (Figure S34). Note that both molar absorptivity coefficients are multiplied by two since per each molecule of **pp-bap** there are two actuator units independently if the actuator groups are as *Z*-isomer or *E*-isomer.

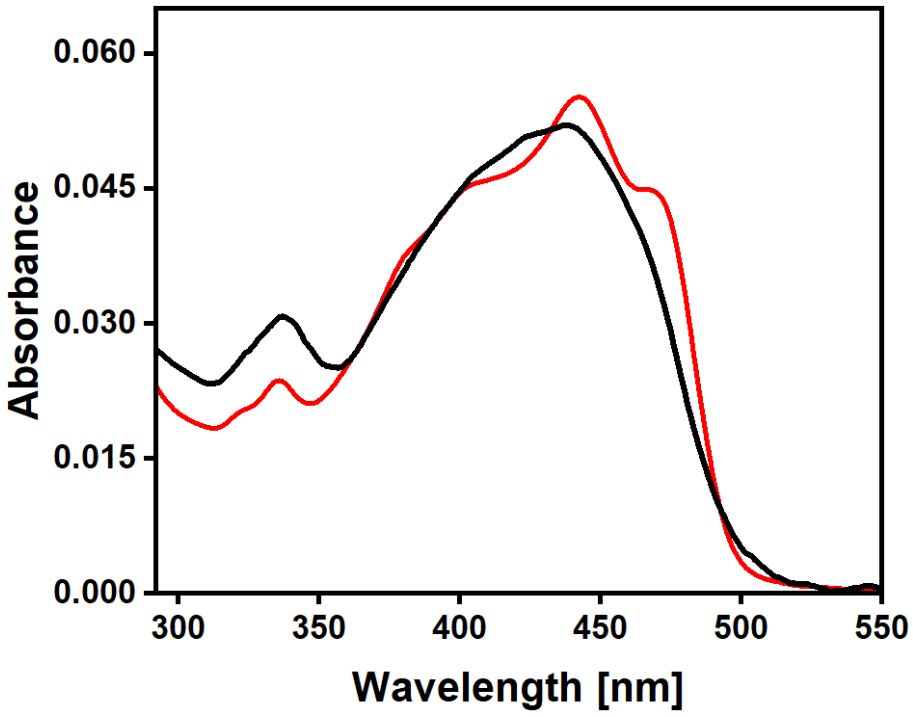

Figure S35. Black line: Absorption spectrum of **pp-bap** after 450 nm irradiation in cyclohexane solution at room temperature. Red line: Spectrum obtained as the algebraic sum of the components of **pp-bap**. From this spectral reconstruction, the overall mole fraction of *Z*-isomers (photo-transformed actuators) can be directly estimated. For the present case it corresponds to 0.42.

Determination of two-photon cross section of pp-bap

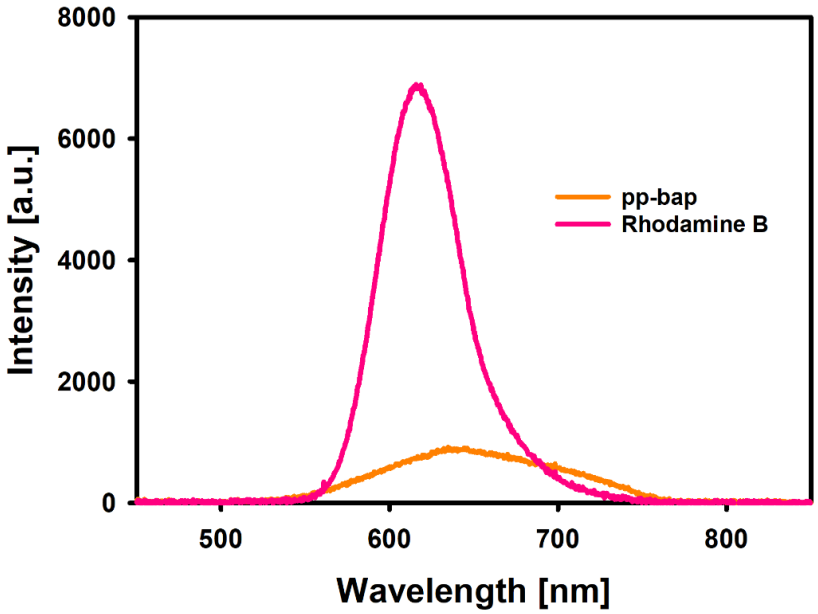

Figure S36. Orange line: emission from a 1.9 x10^{-5} M solution of **pp-bap** in a cyclohexane-chloroform 0.55:0.45 mole fraction mixture after 810 nm biphotonic excitation. Pink line: emission spectrum from a Rhodamine[4] solution in methanol at a concentration of 1 x10^{-6} M which was used as the standard to determine the biphotonic absorption coefficient for **pp-bap**. Both measurements were taken back-to-back with the same excitation irradiance of 4.7 GW/cm^2. The concentrations were adjusted to have both emission signals in the same scale of the detector.

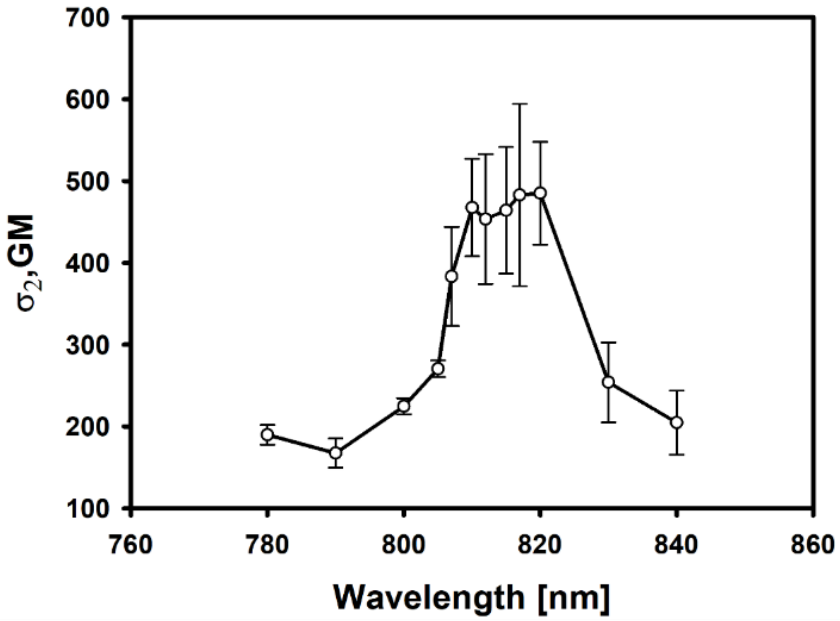

Figure S37. Two-photon absorption cross sections as a function of excitation wavelength for **pp-bap** in a cyclohexane-chloroform 0.55:0.45 mole fraction mixture.

Thermal equilibration of the antenna-actuator systems after biphotonic excitations

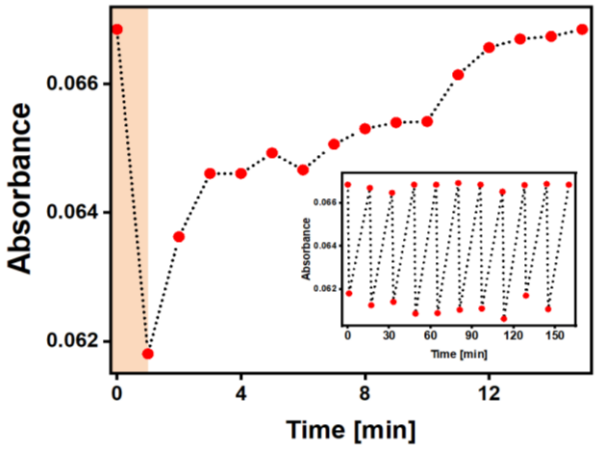

Figure S38. Biphotonic phototransformation of **pp-bap** in cyclohexane solution measured at 413 nm at room temperature upon 800 nm pulsed irradiation at 200 mW average power (24 GW/cm^2) for 1.0 minute. The orange rectangle corresponds to the irradiation time. The inset exhibits various cycles of phototransformations and the back-thermal transformations.

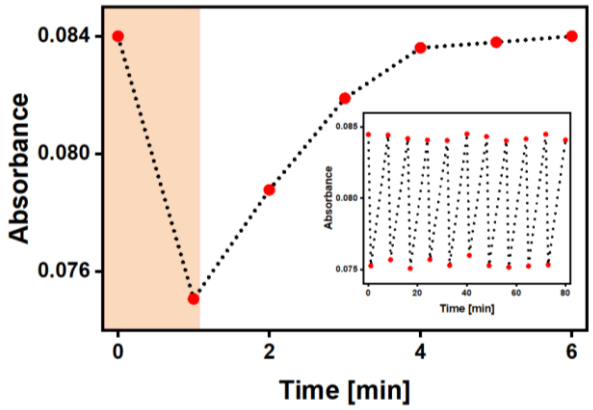

Figure S39. Biphotonic phototransformation of **pp-3sap** in toluene solution measured at 438 nm at room temperature upon 800 nm pulsed irradiation at 150 mW average power (18 GW/cm^2) for 1.0 minute. The orange rectangle corresponds to the irradiation time. The inset exhibits various cycles of phototransformations and the back-thermal transformations.

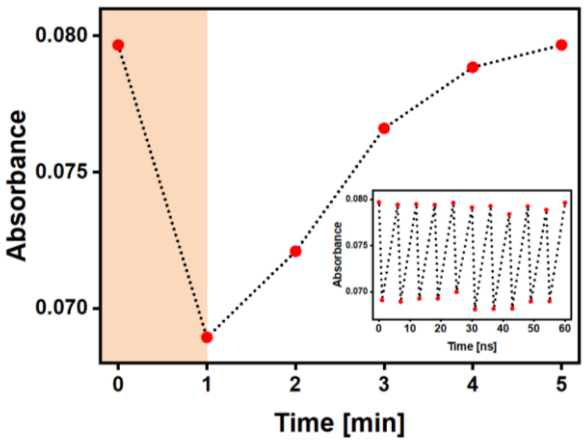

Figure S40. Biphotonic phototransformation of **pp-4sap** in toluene solution measured at 440 nm at room temperature upon 800 nm pulsed irradiation at 150 mW average power (18 GW/cm^2) for 1.0 minute. The orange rectangle corresponds to the irradiation time. The inset shows various cycles of phototransformations and the back-thermal transformations.

Phototransformations of Actuator-Models

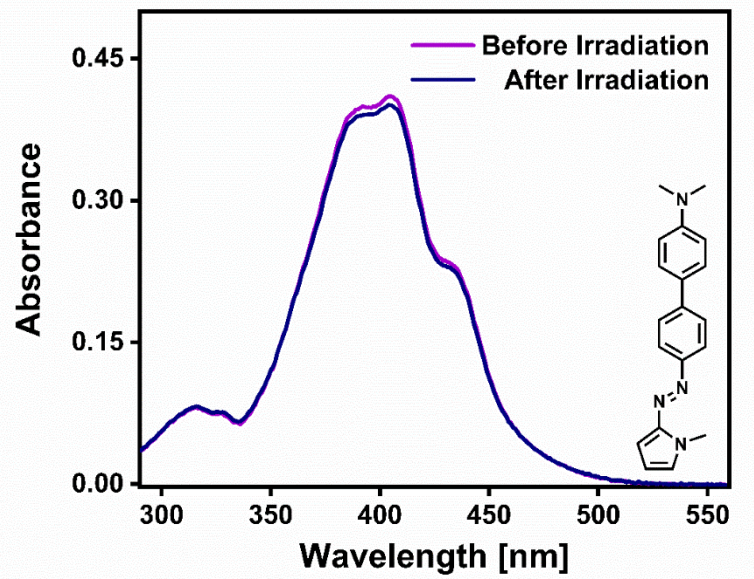

Figure S41. Absorption Spectra of **N-bap** and its molecular structure upon 2PA irradiation at 800 nm for 5 minutes at 45 GW/cm^2 in cyclohexane solution.

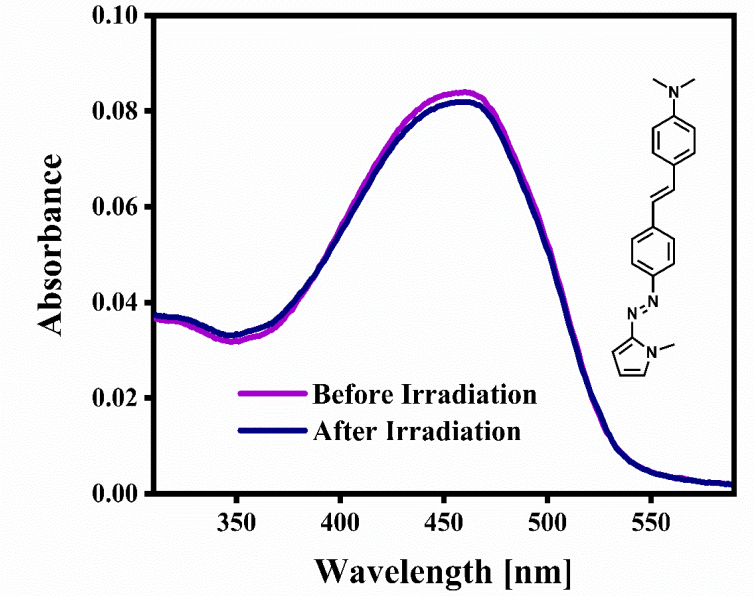

Figure S42. Absorption Spectra of **N-bap** upon 2PA irradiation at 800 nm for 5 minutes at 45 GW/cm^2 in toluene solution.

References

1 M, Tasior, B. Koszarna, D. C. Young, B. Bernard, D. Jaquemin and D. T. Gryko. *Org. Chem. Front.*, 2019, ***6***, 2939–2948.

2 Y. M. Poronik, G. V. Baryshnikov, I. Deperasińska, E. M. Espinoza, J. A. Clark, H. Ågren, D. T. Gryko and V. I. Vullev. *Chem. Commun.*, 2020, ***3***, 1−18.

3 J. Calbo, C. E. Weston, A. J. P. White, H. S. Rzepa, J. Contreras-García and M. Fuchter. *J. Am. Chem. Soc.*, 2017, ***139***, 1261−1274.

4 C. A. Guarin, L. G. Mendoza-Luna, E. Haro-Poniatowski and J. L. Hernández-Pozos. *Spectrochim. Acta A Mol. Biomol. Spectrosc*., 2021, ***249***, 119291.

Full references 61 and 62 of the main article.

61. K. Aidas, C. Angeli, K. L. Bak, V. Bakken, R. Bast, L. Boman, O. Christiansen, R. Cimiraglia, S. Coriani, P. Dahle, E. K. Dalskov, U. Ekström, T. Enevoldsen, J. J. Eriksen, P. Ettenhuber, B. Fernández, L. Ferrighi, H. Fliegl, L. Frediani, K. Hald, A. Halkier, C. Hättig, H. Heiberg, T. Helgaker, A. C. Hennum, H. Hettema, E. Hjertenæs, S. Høst, I.-M. Høyvik, M. F. Iozzi, B. Jansik, H. J. Aa. Jensen, D. Jonsson, P. Jørgensen, P. Kauczor, S. Kirpekar, T. Kjærgaard, W. Klopper, S. Knecht, R. Kobayashi, H. Koch, J. Kongsted, A. Krapp, K. Kristensen, A. Ligabue, O. B. Lutnæs, J. I. Melo, K. V. Mikkelsen, R. H. Myhre, C. Neiss, C. B. Nielsen, P. Norman, J. Olsen, J. M. H. Olsen, A. Osted, M. J. Packer, F. Pawlowski, T. B. Pedersen, P. F. Provasi, S. Reine, Z. Rinkevicius, T. A. Ruden, K. Ruud, T. A. Rybkin, P. Salek, C. C. M. Samson, A. Sánchez de Merás, T. Saue, S. P. A. Sauer, B. Schimmelpfennig, K. Sneskov, A. H. Steindal, K. O. Sylvester-Hvid, P. R. Taylor, A. M. Teale, E. I. Tellgren, D. P. Tew, A. J. Thorvaldsen, L. Thøgersen, O. Vahtras, M. A. Watson, D. J. D. Wilson, M. Ziolkowski and H. Ågren. The Dalton quantum chemistry program system. *Wiley Interdiscip. Rev. Comput. Mol. Sci*, 2014, ***4***, 269–284.

62. M. J. Frisch, G. W. Trucks, H. B. Schlegel, G. E. Scuseria, M. A. Robb, J. R. Cheeseman, G. Scalmani, V. Barone, B. Mennucci, G. A. Petersson, H. Nakatsuji, M. Caricato, X: Li, H. P. Hratchian, A. F. Izmaylov, J. Bloino, G. Zheng, J. L. Sonnenberg, M. Hada, M. Ehara, K. Toyota, R. Fukuda, J. Hasegawa, M. Ishida, T. Nakajima, Y. Honda, O. Kitao, H. Nakai, T. Vreven, J. A. Montgomery Jr., J. E. Peralta, F. Ogliaro, M. Bearpark, J. J. Heyd, E. Brothers, K. N. Kudin, V. N. Staroverov, R. Kobayashi, J. Normand, K. Raghavachari, A. Rendell, J. C. Burant, S. S. Iyengar, J. Tomasi, M.

Cossi, N. Rega, J. M. Millam, M. Klene, J. E. Knox, J. B. Cross, V. Bakken, C. Adamo, J. Jaramillo, R. Gomperts, R. E. Stratmann, O. Yazyev, A. J. Austin, R. Cammi, C. Pomelli, J. W. Ochterski, R. L. Martin, K. Morokuma, V. G. Zakrzewski, G. A. Voth, P. Salvador, J. J. Dannenberg, S. Dapprich, A. D. Daniels, O. Farkas, J. B. Foresman, J. V. Ortiz, J. Cioslowski and D. J. Fox. *Gaussian* 16, revision A.03; Gaussian, Inc.: Wallingford, CT, 2016.